RSC Applied Polymers

ROYAL SOCIETY OF CHEMISTRY

REVIEW

View Article Online
View Journal | View Issue

Cite this: *RSC Appl. Polym.*, 2024, **2**, 996

A new way to improve the fire safety of polyurethane composites with the assistance of metal–organic frameworks

Jinhu Hu,[a] Ye-Tang Pan, *[a] Keqing Zhou, *[b] Pingan Song[c,d] and Rongjie Yang[a]

Polyurethane (PU) is extensively utilized for its outstanding properties. However, its flammability and the substantial release of toxic smoke and harmful gases during combustion pose significant safety concerns in practical applications. Consequently, the development of efficient flame-retardant PU materials has become a critical priority. In recent years, metal–organic frameworks (MOFs) have attracted considerable interest as innovative flame retardants. Thanks to their structural diversity, large specific surface area, tunable porosity, and multifunctional properties, MOF materials show significant promise in improving the flame retardancy of PU. MOFs not only catalyze the formation of stable char layers during PU combustion but also adsorb and trap smoke and toxic gases, all while avoiding the release of corrosive or toxic gases at high temperatures, unlike conventional flame retardants. This review systematically compiles the latest progress in using MOFs to enhance PU flame retardancy, with an emphasis on their applications in polyurethane elastomers (PUE), thermoplastic polyurethanes (TPU), and polyurethane foams (PUF). This paper offers a comprehensive evaluation of the flame-retardant effects of various MOF structures and investigates the synergistic interactions between MOFs and other flame retardants. Additionally, this work identifies current challenges and future development paths, offering theoretical guidance and research avenues for advancing efficient and safe flame-retardant PU materials. This is crucial for enhancing the safety of PU materials and broadening their application areas.

Received 19th August 2024,
Accepted 24th September 2024

DOI: 10.1039/d4lp00257a

rsc.li/rscapplpolym

1. Introduction

Polyurethane (PU) is a polymer synthesized by reacting isocyanates (R–N=C=O) with active hydrogen-containing compounds (polyols).[1–3] The synthesis principle is illustrated in Fig. 1. The –NCO groups of isocyanates (*e.g.*, MDI, TDI) react with the –OH groups of polyols (*e.g.*, polyether polyols, polyester polyols) to form urethane bonds (–NHCOO–), resulting in the formation of PU chains.[4,5] The molecular weight and properties of PU can be adjusted by controlling chain growth and crosslinking reactions. PU exhibits excellent wear resistance, corrosion resistance, chemical resistance, and elastic recovery, making it widely used in furniture, automotive, construction, and electronics industries.[6] However, due to its physical and chemical properties, PU is inherently flammable. Consequently, developing PU flame retardants is crucial for slowing the combustion process, reducing smoke and toxic gases emissions, and decreasing fire risks, thus enhancing overall safety.

Metal–organic frameworks (MOFs) are a novel class of porous nanomaterials created through the coordination of metal ions or clusters with organic ligands.[7,8] By selecting specific metal ions and organic ligands, MOFs can be tailored into various structures, from one-dimensional (1D) chains to three-dimensional (3D) channels.[9,10] MOFs typically possess very high specific surface areas (theoretically up to 14 600 $m^2 g^{-1}$) and rich pore structures.[11] These characteristics enable MOFs to exhibit exceptional performance in areas such as adsorption and catalysis. Consequently, MOFs have demon-

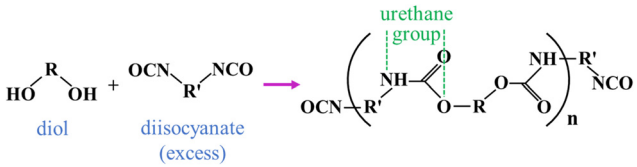

Fig. 1 Reaction scheme of preparing PU.

[a]*National Engineering Research Center of Flame Retardant Materials, School of Materials Science & Engineering, Beijing Institute of Technology, Beijing 100081, PR China. E-mail: pyt@bit.edu.cn*
[b]*Faculty of Engineering, China University of Geosciences (Wuhan), Wuhan, Hubei 430074, PR China. E-mail: zhoukq@cug.edu.cn*
[c]*School of Agriculture and Environmental Science, University of Southern Queensland, Springfeld Central, QLD 4300, Australia*
[d]*Centre for Future Materials, University of Southern Queensland, Springfeld Central, QLD 4300, Australia*

strated broad application potential in fields like catalysis, medicine, separation, and sensing.[12–15] In recent years, MOFs have garnered significant attention in the development of flame retardant materials.[16] During combustion, MOFs can catalyze the formation of a dense char layer on the polymer surface, serving as a protective barrier.[17] Moreover, their porous structure is effective in adsorbing and trapping smoke and toxic gases produced during combustion. Compared to traditional halogen-containing flame retardants, MOF materials do not produce corrosive or toxic hydrogen halide gases at high temperatures.[18] MOFs provide a wide range of design and functionalization options. Modifying the metal centers or organic ligands allows for the precise control of pore size, surface chemical properties, and thermal stability in MOF materials, enabling the design of materials with specific flame-retardant characteristics.[19]

Recently, MOF-based materials have been extensively studied for their flame-retardant properties in polymers like PU, epoxy resins (EP),[20,21] and polystyrene (PS).[22,23] Hou *et al.*[24] were the first to propose the idea of incorporating MOFs as flame retardants into PS, demonstrating the feasibility of MOF-based flame retardants. Song *et al.*[25] utilized ZIF-67 as a carrier, integrating triphenyl phosphate (TPP), cobalt–cobalt layered double hydroxide (CoCo-LDH), and cobalt basic carbonate (CBC) to construct a novel bird's nest-like nanostructure (m-CBC-P@LDH). Incorporating 5 wt% m-CBC-P@LDH into polyurea (PUA) composites led to a 41.7% reduction in peak heat release rate (pHRR) and a 20.6% decrease in total heat release (THR), with minimal impact on mechanical properties. Han *et al.*[26] developed an organic phosphorus-modified MOF with a distinctive hierarchical porous nanostructure (P-Co-MOF/ZIF) for flame retardancy in EP. The inclusion of 2 wt% P-Co-MOF/ZIF in EP led to reductions of 43.3%, 37.9%, and 38.1% in pHRR, THR, and total smoke production (TSP), respectively. Despite notable advances in the polymer flame retardant field with MOF-based materials, their application in various types of PU, especially in polyurethane elastomers (PUE), thermoplastic polyurethane (TPU), and rigid/soft polyurethane foams (RPUF/FPUF), is still underexplored. Fig. 2 summarizes the development trends of MOF-based PU flame retardants in recent years. The figure shows the increase in the number of publications related to this field over time, reflecting that the application of MOFs in PU flame retardant materials is gradually becoming a research hotspot. As more studies highlight the excellent flame retardant properties of MOFs, particularly in enhancing the thermal stability and smoke suppression of PU, it is expected that research in this area will continue to grow in the future. This review seeks to systematically summarize recent advancements in enhancing PU flame retardancy using MOF-based materials. Through a comprehensive review of existing research, we aim to elucidate the advantages and challenges of MOF-based flame retardants in PU, offering theoretical support and guiding future research directions for the development of flame-retardant PU materials.

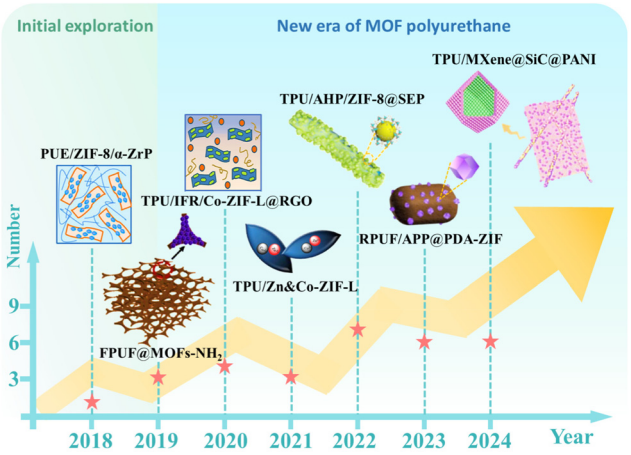

Fig. 2 Development trend of MOF-based flame retardant PU in recent years (until August 2024).

2. Flame retardant performance and mechanisms of MOFs

2.1 Characterization methods

To comprehensively evaluate the flame retardancy of MOF-based PU composites, it is essential to use multiple characterization techniques. The cone calorimeter test (CCT), limiting oxygen index (LOI), and UL-94 vertical burning test are the three most commonly used methods for assessing bench scale testing of flame retardancy, and screening of flame retardant potential in regulatory tests.

CCT is a dynamic test method that simulates the combustion behavior of materials in real fire scenarios. This technique applies a fixed radiant heat flux to the material and records various combustion parameters, including pHRR, THR, TSP, peak smoke production rate (pSPR), and the total release of CO and CO_2 during combustion (TCOP, TCO_2P). CCT can comprehensively evaluate the combustion characteristics of materials, making it a core tool for studying flame-retardant material performance under laboratory conditions. LOI is a static and straightforward method that measures the minimum concentration of oxygen required to sustain the combustion of a material. Expressed as a percentage, a higher LOI value indicates greater resistance to burning in air, meaning the material has better flame retardant properties. The UL-94 test is one of the most widely used methods for classifying the flammability of materials, particularly in a vertical burning configuration. This test evaluates the self-extinguishing behavior and dripping characteristics of materials when burned. Materials are categorized into different ratings (such as V-0, V-1, and V-2), with V-0 being the highest rating, indicating that the material self-extinguishes within 10 s without producing flaming drips after two 10-second burn cycles.

However, these testing methods are primarily used for preliminary evaluations under laboratory conditions and may not fully represent large-scale fire scenarios in real-world appli-

cations. Each method has its limitations. For instance, CCT mainly measures the heat release characteristics of materials, but it may not fully capture the material's behavior in a complex fire environment. While LOI test provides data on how materials burn under varying oxygen concentrations, it does not account for other potential factors encountered in practical applications. The UL-94 test focuses on the material's self-extinguishing properties, but its results may not be sufficient to comprehensively reflect material performance in real fire scenarios. Therefore, for practical applications, it is necessary to combine these methods with other more comprehensive fire testing approaches to further verify the flame retardant performance of materials.

2.2 Flame retardant and smoke suppression mechanism of MOFs

The flame-retardant properties of MOF materials are derived from both condensed-phase and gas-phase mechanisms. During combustion, transition metals within MOFs function as Lewis acids, catalyzing the decomposition and carbonization of the matrix material.[27] These metals reduce the decomposition temperature of polymers at elevated temperatures, promoting the formation of a stable char layer and decreasing the production of flammable gases.[28] The resulting char layer effectively insulates the material from O_2 and heat, thereby inhibiting further combustion.[29] Additionally, metal ions such as Co, Zn, Cu, and Zr in certain MOFs can enhance the carbonization process at elevated temperatures, improving the quality and stability of the char layer, thereby enhancing flame retardancy.[30–33] Furthermore, MOF materials can release non-flammable gases (such as water vapor and CO_2), at elevated temperatures, which dilute the concentration of flammable gases in the combustion zone, thereby lowering the flame temperature.[34]

The organic–inorganic hybrid structure of MOFs provides possibilities for designing novel functionalized flame retardants. Organic ligands in MOFs can improve compatibility with polymer chains, while their organic structure facilitates the introduction of flame-retardant groups like P, N, and aromatic groups.[35–37] Additionally, MOF materials can be integrated with other flame retardants (*e.g.*, phosphorus-based and silicon-based) to boost the overall effectiveness of the flame-retardant system.[38] MOF materials can uniformly disperse within the matrix, offering more active sites and thereby enhancing flame retardant performance.[39,40]

MOF-derived metal oxides, such as CuO, Co_3O_4, CoO, and β-$Fe(OH)_3$, are highly efficient smoke-suppressing catalysts. This effectiveness stems from the ability of metal ions to form catalytic metal oxides at high temperatures, which can capture free radicals (*e.g.*, carbon radicals) generated in the flame, thereby inhibiting the formation of soot particles and reducing smoke production.[41,42] Owing to their distinctive pore structure and surface chemistry, MOF materials are highly effective in adsorbing and immobilizing toxic gases like HCl, HCN, and nitrogen oxides (NO_x) generated during combustion.[43] The metal ions or functionalized organic ligands within MOFs can physically or chemically adsorb these toxic gas molecules, reducing their release into the atmosphere.

3. MOF in polyurethane for fire retardant

3.1 Polyurethane elastomers (PUE)

PUE is widely utilized in industries like automotive (*e.g.*, seals and gaskets), footwear (*e.g.*, shoe soles), and industrial belts due to its excellent elasticity, radiation resistance, wear resistance, and low-temperature resilience.[44] However, PUE is susceptible to combustion in air, leading to the release of toxic gases such as HCN and CO, which pose significant risks to human health and the environment.[45] Incorporating MOFs can improve the flame retardancy of polymer materials. Xu *et al.*[46] synthesized a novel flame retardant by modifying α-zirconium phosphate (α-ZrP) with zeolitic imidazolate frameworks-8 (ZIF-8), as illustrated in Fig. 3(a–f). Test results indicate that the ZIF-8/α-ZrP/PUE composite containing 2 wt% flame retardant exhibits higher char yield and an increased glass transition temperature (T_g) at 700 °C compared to pure PUE. The pHRR, THR, pSPR, and TSP of the ZIF-8/α-ZrP/PUE composite material, with a thickness of 4.0 mm (heat flux of 50 kW m^{-2}), decreased by 69.6%, 45.6%, 59.3%, and 40.5%, respectively (see Fig. 3(g–j)). The enhancement in flame retardancy and smoke suppression is primarily due to the physical barrier and catalytic carbonization effects of α-ZrP. Wang *et al.*[47] explored the effect of combining ZIF-8 with expandable graphite (EG) on the flame retardancy of PUE. The findings revealed that with a flame retardant content of 3 wt% (with a ZIF-8 to EG ratio of 1 : 3), the ZIF-8/EG/PUE composite demonstrated optimal flame retardant and smoke suppression performance. Compared to pure PUE, the pHRR, THR, maximum smoke density ($D_{s,max}$), and smoke density at 10 minutes ($D_{10,min}$) of the ZIF-8/EG/PUE composite decreased by 83.4%, 42.6%, 22.4%, and 28.3% (3.0 mm thickness, heat flux of 50 kW m^{-2}), respectively, as illustrated in Fig. 3(l–n). LOI of the ZIF-8/EG/PUE composite, tested at a thickness of 3.0 mm, increased to 30.2% (Fig. 3(o)), and the UL-94 vertical burning test achieved a V-1 rating (Fig. 3(k)).

3.2 Thermoplastic polyurethane (TPU)

TPU is a linear PU structure made up of soft and hard segments connected through physical cross-linking. The hard segments are typically formed by diisocyanates and chain extenders (such as diols), while the soft segments consist of high molecular weight polyols.[48] Due to this linear structure, TPU can soften upon heating and re-solidify upon cooling, exhibiting reversible thermoplastic properties. As a result, TPU demonstrates reversible thermoplasticity, excellent elasticity, and processability. Due to these properties, TPU finds widespread applications in flexible films, hoses, cable insulation, medical equipment and consumer electronics.[49] However, TPU is highly flammable and decomposes rapidly under fire, emitting significant quantities of toxic and harmful smoke.[50,51]

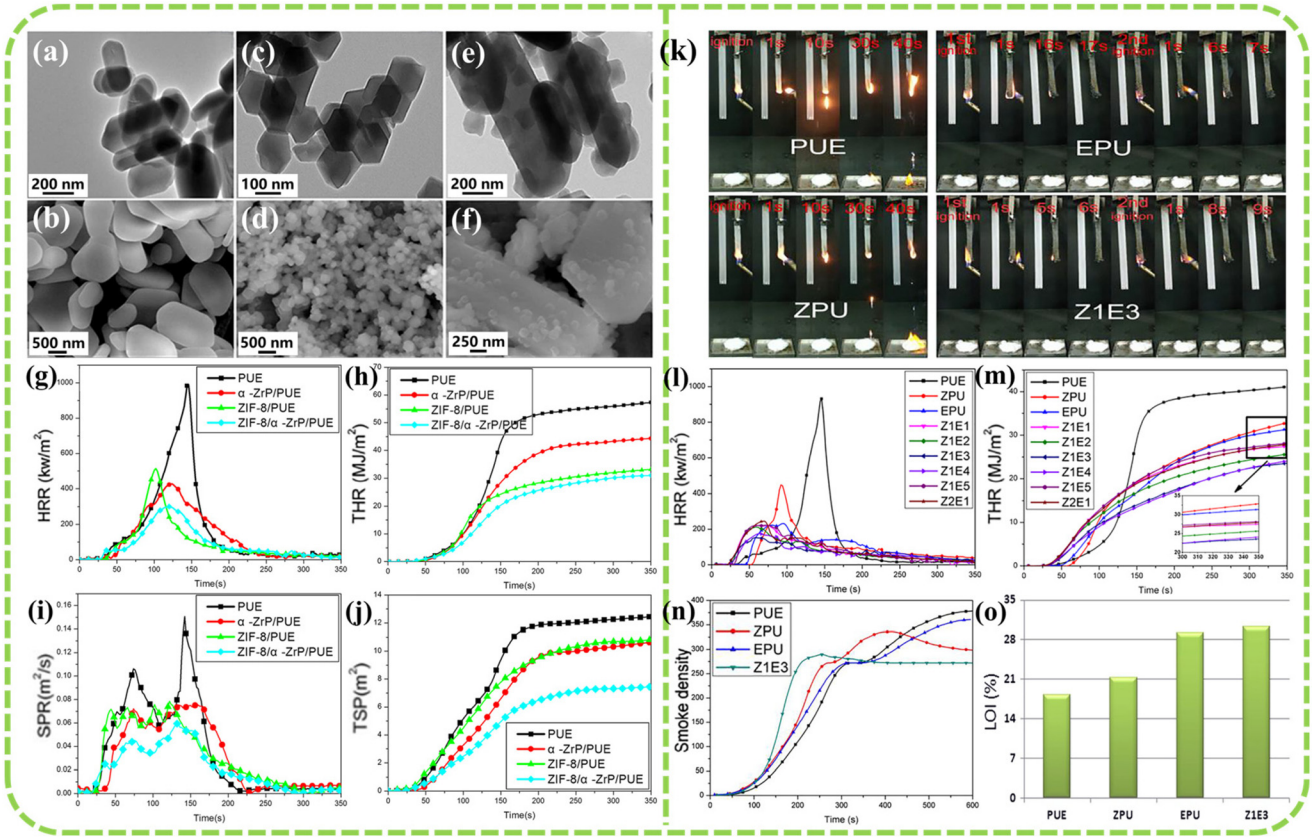

Fig. 3 TEM and SEM images of (a and b) α-ZrP, (c and d) ZIF-8, and (e and f) ZIF-8/α-ZrP; (g) HRR, (h) THR, (i) SPR and (j) TSP curves. Reproduced with permission from ref. 46, copyright reserved Wiley 2018. (k) UL-94 vertical burning test; (l) HRR, (m) THR, (n) smoke density, and (o) LOI curves for pure PUE and PUE composites (Z_xE_y denotes the ZIF-8 to EG ratio of $x:y$). Reproduced with permission from ref. 47, copyright reserved Wiley 2019.

Thus, it is crucial to design TPU with enhanced flame retardant and smoke suppression capabilities.

Xu *et al.*[52] used an eco-friendly method to synthesize three types of two-dimensional (2D) nanosheets: Zn-ZIF-L, Co-ZIF-L, and Zn&Co-ZIF-L. These nanosheets were each incorporated into TPU at a 3 wt% loading to evaluate their effectiveness in improving TPU's flame retardancy and smoke suppression. The flame retardant performance of the three MOF composites is detailed in Table 1, where all three nanosheets exhibited excellent flame retardant and smoke suppression capabilities. Li *et al.*[53] developed an innovative ZIF-8@SEP hybrid nanoparticle, serving as both a synergistic flame retardant and coupling agent in TPU/aluminum hypophosphite (AHP) composites. The TPU composite with 8.0 wt% AHP and 1.0 wt% ZIF-8@SEP reached an LOI of 27.5%, conforming to the UL-94 V-0 rating. Compared to the TPU, pHRR, THR, pSPR, and TSP were reduced by 78.9%, 39.1%, 44.1%, and 9.0%, respectively. The incorporation of flame retardant fillers caused only a slight reduction in tensile strength and elongation at break by 2.0% and 7.8%, suggesting a minimal impact on mechanical properties. Wu *et al.*[54] used an electrostatic technique to layer-by-layer self-assemble negatively charged phytic acid (PA) and positively charged hyperbranched polysiloxane (NH_2-HBPSi) onto ZIF-8, forming a core–shell structure. Compared to pure TPU, the composite with 2.0 wt% ZIF-8@PA@NH_2-HBPSi showed reductions in pHRR, THR, pSPR, TSP, peak CO production rate (pCOP), and peak CO_2 production rate (pCO_2P) by 35.2%, 25.2%, 21.4%, 65.5%, 30.8%, and 37.2%, respectively. Additionally, the TPU/ZIF-8@PA@NH_2-HBPSi composite achieved an elongation at break of 2178.2% and a tensile strength of 46.87 MPa, reflecting an enhancement in mechanical properties. To utilize industrial solid waste fully and tackle water eutrophication, Tu *et al.*[55] used a phosphate-adsorbing composite material (MH@MOF-P) as an effective flame retardant for TPU. This method not only allowed for waste recycling and water purification but also promoted the sustainable use of phosphate adsorption products in flame-retardant polymer materials. Specifically, flower-like magnesium hydroxide (MH) was synthesized from phosphate tailings and then coated with Zn-MOF to produce MH@MOF. This material was used to adsorb phosphate from wastewater, yielding MH@MOF-P, which was then incorporated into TPU through solution blending. The results showed that compared to pure TPU, the TPU containing 4 wt% MOF@MH-P exhibited substantial reductions in pHRR, pSPR, TSR, pCOP, and pCO_2P by 45.8%, 46.7%, 21.4%, 37.4%, and 50.0%, respectively.

Table 1 Flame retardant properties of MOF composite TPU compared to pure TPU

Type of FRs	Loading (wt%)	LOI/*T* (%/mm)	UL-94/*T* (mm)	Main flame-retardant results/*T* (mm)	Ref.
Zn-ZIF-L	3.0	25.3/4.0	—	3/28.8%, 7.8%, 50.0%, 18.5%, 37.5% and 13.4% reduction in pHRR, THR, pSPR, TSP, pCOP and pCO_2P/3.0 (heat flux of 50 kW m^{-2})	52
Co-ZIF-L	3.0	26.0/4.0	—	42.8%, 11.4%, 45.0%, 18.5%, 50.0% and 26.9% reduction in pHRR, THR, pSPR, TSP, pCOP and pCO_2P/3.0 (heat flux of 50 kW m^{-2})	
Zn&Co-ZIF-L	3.0	25.7/4.0	—	43.8%, 9.3%, 51.5%, 22.9%, 50.0% and 20.9% reduction in pHRR, THR, pSPR, TSP, pCOP and pCO_2P/3.0 (heat flux of 50 kW m^{-2})	
AHP/ZIF-8@SEP	8.0/1.0	27.5%/3.0	V-0/3.0	78.9%, 39.1%, 44.1% and 9.0% reduction in pHRR, THR, pSPR and TSP/3.0 (heat flux of 50 kW m^{-2})	53
ZIF-8@PA@NH_2-HBPSi	2.0	—	—	35.2%, 25.2%, 21.4%, 65.5%, 30.8%, 37.2%, 52.8% and 25.2% reduction in pHRR, THR, pSPR, TSP, pCOP, pCO_2P, TCOP and TCO_2P/3.0 (heat flux of 35 kW m^{-2})	54
MH@MOF-P	4.0	—	—	45.8%, 46.7%, 21.4%, 37.4% and 50.0% reduction in pHRR, pSPR, TSP, pCOP and pCO_2P/3.0 (heat flux of 35 kW m^{-2})	55
Co-ZIF-L@RGO/IFR	3.0/27.0	32.6	V-0	84.4%, 70.1%, 60.3%, 62.5%, 80.9%, 92.5% reduction in pHRR, THR, pSPR, TSP, pCOP and pCO_2P/6.0	56
NiCo-LDH/MoS_2	2	—	—	42.9%, 10.7%, 55.7% and 33.3% reduction in pHRR, THR, pSPR and TSP/3.0 (heat flux of 50 kW m^{-2})	57
ZIF-67 H	2	—	—	45.4%, 10.1%, 71.3%, 50.2%, 45.5% and 9.1% reduction in pHRR, THR, pSPR, TSP, TCOP and TCO_2P/3.0 (heat flux of 35 kW m^{-2})	58
APP/Co-MOF	4.5/1.5	28.2/3.0	V-0/3.0	81.1%, 19.2%, 63.6% and 31.1% reduction in pHRR, THR, pSPR and TSP/3.0 (heat flux of 50 kW m^{-2})	61
APP/MOF-Cu	7.9375/0.0625	27.0/3.2	V-0/3.2	76.0%, 69.3%, 58.9%, 77.8%, 44.3% and 75.5% reduction in pHRR, THR, pSPR, TSP, pCOP and pCO_2P/3.0 (heat flux of 35 kW m^{-2})	62
APP/ZIF-67@GO	6.5/0.5	27.4/3.0	V-0/3.0	81.2%, 29.0%, 48.7%, 24.3%, 72.5% and 87.3% reduction in pHRR, THR, pSPR, TSP, pCOP and pCO_2P/3.0 (heat flux of 50 kW m^{-2})	63
APP@SiO_2@UiO-66-NH_2(Zr)	20	29.9	—	75.1%, 87.8%, 63.6%, 87.7%, 52.4% and 76.8% reduction in pHRR, THR, pSPR, TSP, pCOP and pCO_2P/3.0 (heat flux of 35 kW m^{-2})	64
APP@UiO-66-NH_2(Zr)	20	—	—	75.76%, 86.19%, 69.74%, 86.34%, 57.14% and 76.37% reduction in pHRR, THR, pSPR, TSP, pCOP and pCO_2P (heat flux of 35 kW m^{-2})	65
GO@NH_2-UIO-66(Zr)	2	28.4	V-0	74.6%, 35.0%, 64.3% and 68.9% reduction in pHRR, THR, pSPR and TSP/3.0	66
Ni-MOF@$Ti_3C_2T_x$	2	—	—	19.5%, 3.3%, 35.3%, 22.9%, 25.4% and 13.3% reduction in pHRR, THR, pSPR, TSP, pCOP and pCO_2P/3.0 (heat flux of 35 kW m^{-2})	71
Co-MOF@MXene	2	—	—	28.3%, 14.5%, 58.8%, 47.5%, 57.7% and 35.9% reduction in pHRR, THR, pSPR, TSP, pCOP and pCO_2P/3.0 (heat flux of 35 kW m^{-2})	72
MXene@SiC@PANI	5	26.2/3.0		71.4%, 34.6%, 72.8%, 49.1%, 72.3% and 78.8% reduction in pHRR, THR, pSPR, TSP, pCOP and pCO_2P (heat flux of 50 kW m^{-2})	73
APP-PEI@MXene@ZIF-67-2BL	20	—	—	72.75%, 87.25%, 59.58%, 85.97%, 29.1% and 74.5% reduction in pHRR, THR, pSPR, TSP, pCOP and pCO_2P (heat flux of 35 kW m^{-2})	74

T represents thickness. If *T* and heat flux are not indicated, the reference does not provide data.

Xu *et al.*[56] developed a novel leaf-like Co-ZIF modified reduced graphene oxide hybrid (Co-ZIF-L@RGO) and combined it with an intumescent flame retardant (IFR). The composite was incorporated into TPU to study the effects of the Co-ZIF-L@RGO and IFR combination on TPU's thermal conductivity and flame retardant properties. Results indicated that compared to pure TPU, the pHRR, THR, pSPR and TSP of the composites (with 3 wt% Co-ZIF-L and 27 wt% IFR) decreased by 84.4%, 70.1%, 60.3% and 62.5%, respectively. Qian *et al.*[57] used ZIF-67 as a template to synthesize a novel 3D hollow nickel-cobalt layered double hydroxide (NiCo-LDH). The 3D hollow NiCo-LDH was assembled onto MoS_2 nanosheets *via* electrostatic self-assembly, forming a 3D hollow NiCo-LDH/MoS_2 hybrid material. Compared to pure TPU, the TPU composite with 2 wt% NiCo-LDH/MoS_2 showed reductions in pHRR, THR, pSPR, and TSP by 42.9%, 10.7%, 55.7%, and 33.3%, respectively. By adjusting the ratio of 2-methylimidazole to $Co(NO_3)_2{\cdot}6H_2O$ and adding surfactant (CTAB), Geng *et al.*[58] prepared ZIF-67 with dodecahedron (ZIF-67), cube (ZIF-67NC) and cross (ZIF-67H) (see Fig. 4). These structures were used to enhance the flame retardant and smoke suppression properties of TPU. During the combustion of TPU composites, the novel cross-shaped ZIF-67 H exhibited superior catalytic and flame retardant performance compared to the other two forms. This may be due to the unique 3D cross-shaped morphology of ZIF-67 H. Additionally, XPS analysis revealed that more Co elements were exposed on the surface of ZIF-67 H, which could be related to its superior catalytic activity. Compared to pure TPU, the TPU/2 wt% ZIF-67 H composite showed reductions in pHRR, THR, pSPR, TSP, total CO production (TCOP), and total CO_2 production (TCO_2P) by 45.4%, 10.1%, 71.3%, 50.2%, 45.5%, and 9.1%, respectively.

Ammonium polyphosphate (APP) is a highly valuable phosphorus-based flame retardant.[59] However, the poor compatibility between APP and polymers, due to differing polarities, limits its flame-retardant efficiency. Surface modification of APP effectively addresses this issue.[60] Wang *et al.*[61] synthesized

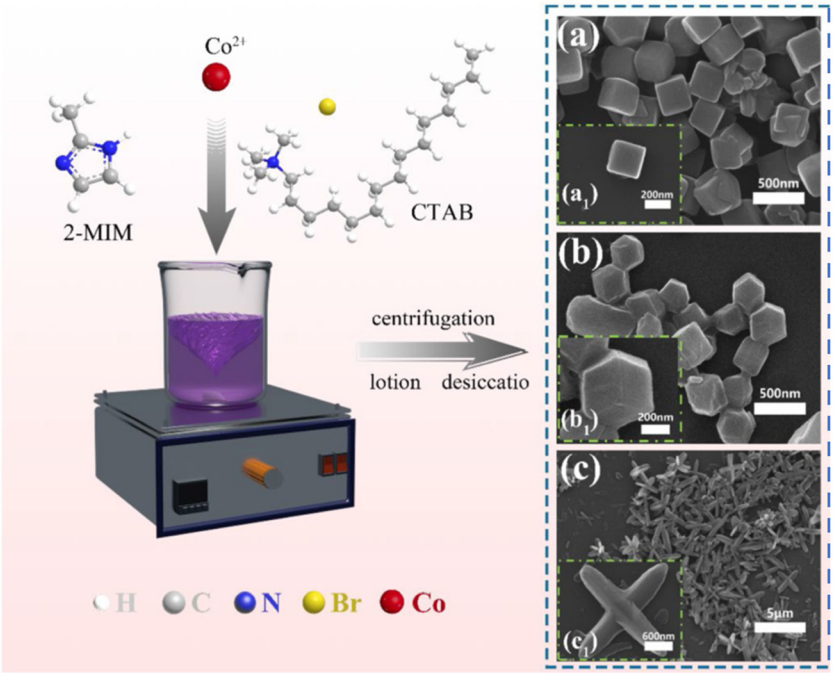

Fig. 4 Preparation procedure and SEM images of (a) ZIF-67 NC, (b) ZIF-67, and (c) ZIF-67 H. Reproduced with permission from ref. 58, copyright reserved Elsevier 2024.

a Co-based MOF (Co-MOF) to modify APP, enhancing the flame retardancy of TPU composites. The TPU composite with 4.5 wt% APP and 1.5 wt% Co-MOF achieved an LOI of 28.2% and a UL-94 V-0 rating. Reductions in pHRR, THR, pSPR, and TSP for the TPU composite were 81.1%, 19.2%, 63.6%, and 31.1%, respectively. Chen *et al.*[62] synthesized a Cu-based MOF (MOF-Cu) and combined it with APP to prepare flame-retardant TPU composites. Compared to pure TPU, the TPU composite with 0.0625 wt% MOF-Cu and 7.9375 wt% APP showed reductions in pHRR, THR, TSP, and pCOP by 76.0%, 69.3%, 77.8%, and 44.2%, respectively. Liu *et al.*[63] hybridized ZIF-67 with graphene oxide (GO) to create ZIF-67@GO, which was then combined with APP to enhance TPU's flame retardancy and smoke suppression. With 6.5 wt% APP and 0.5 wt% ZIF-67@GO, the TPU sample's flame retardancy significantly improved, achieving an LOI of 27.4% and a UL-94 V-0 rating. pHRR, THR, pSPR, TSP, pCOP, and pCO_2P values were reduced by 81.2%, 29.0%, 48.7%, 24.3%, 72.5%, and 87.3%, respectively. Additionally, the flame-retardant TPU had a tensile strength of 18.3 MPa and elongation at break of 1026.3%, meeting industrial application requirements. These studies indicate that the optimal ratio of MOF to APP depends on the specific composition of the materials and their interactions within the TPU matrix. Researchers determine the ideal proportion through experimental testing, which involves evaluating the flame retardancy and mechanical properties of TPU composites containing different MOF and APP combinations. By systematically varying the ratios and measuring key parameters such as HRR, THR, TSP, char formation, and mechanical properties, they can identify the ratio that offers the best balance between flame retardancy and mechanical performance. Moreover, the synergistic effect between MOF and APP typically stems from their complementary flame-retardant mechanisms. APP promotes the formation of an expanded char layer during combustion, acting as a barrier against heat and O_2. MOFs, with their porous structures and catalytic properties, further enhance char formation and help capture and decompose flammable gases. The metal ions in MOFs can catalyze the thermal degradation of the TPU matrix, thereby reducing the generation of flammable gases.

Wan *et al.*[64] developed a multilayer core–shell flame retardant (APP@SiO_2@UiO-66-NH_2(Zr)) by encapsulating APP with UiO-66-NH_2(Zr), tetraethyl orthosilicate, and γ-(2,3-epoxypropoxy) propyltrimethoxysilane, as shown in Fig. 5(a). The TPU composite with 20 wt% APP@SiO_2@UiO-66-NH_2(Zr) showed significant reductions in pHRR, THR, pSPR, TSP, pCOP, and pCO_2P by 75.1%, 87.8%, 63.6%, 87.7%, 52.4%, and 76.8%, respectively, compared to pure TPU. The flame retardant mechanism (Fig. 5(b)) indicates that APP@SiO_2@UiO-66-NH_2(Zr) enhances TPU's flame retardancy through the synergistic action of multiple elements. This includes acting as a physical barrier, catalyzing char formation, inhibiting chain reactions, and releasing non-combustible gases to suppress combustion. Shi *et al.*[65] modified APP with UiO-66-NH_2(Zr) to create a synergistic flame retardant (APP@MOFs). When added to TPU, the composite with 20 wt% APP@MOFs showed significant reductions in pHRR, THR, pSPR, TSP, pCOP, and pCO_2P by 75.76%, 86.19%, 69.74%, 86.34%, 57.14%, and 76.37%, respectively, compared to pure TPU. Yao *et al.*[66] modified NH_2-UIO-66(Zr) with SiO_2, multi-walled carbon nanotubes

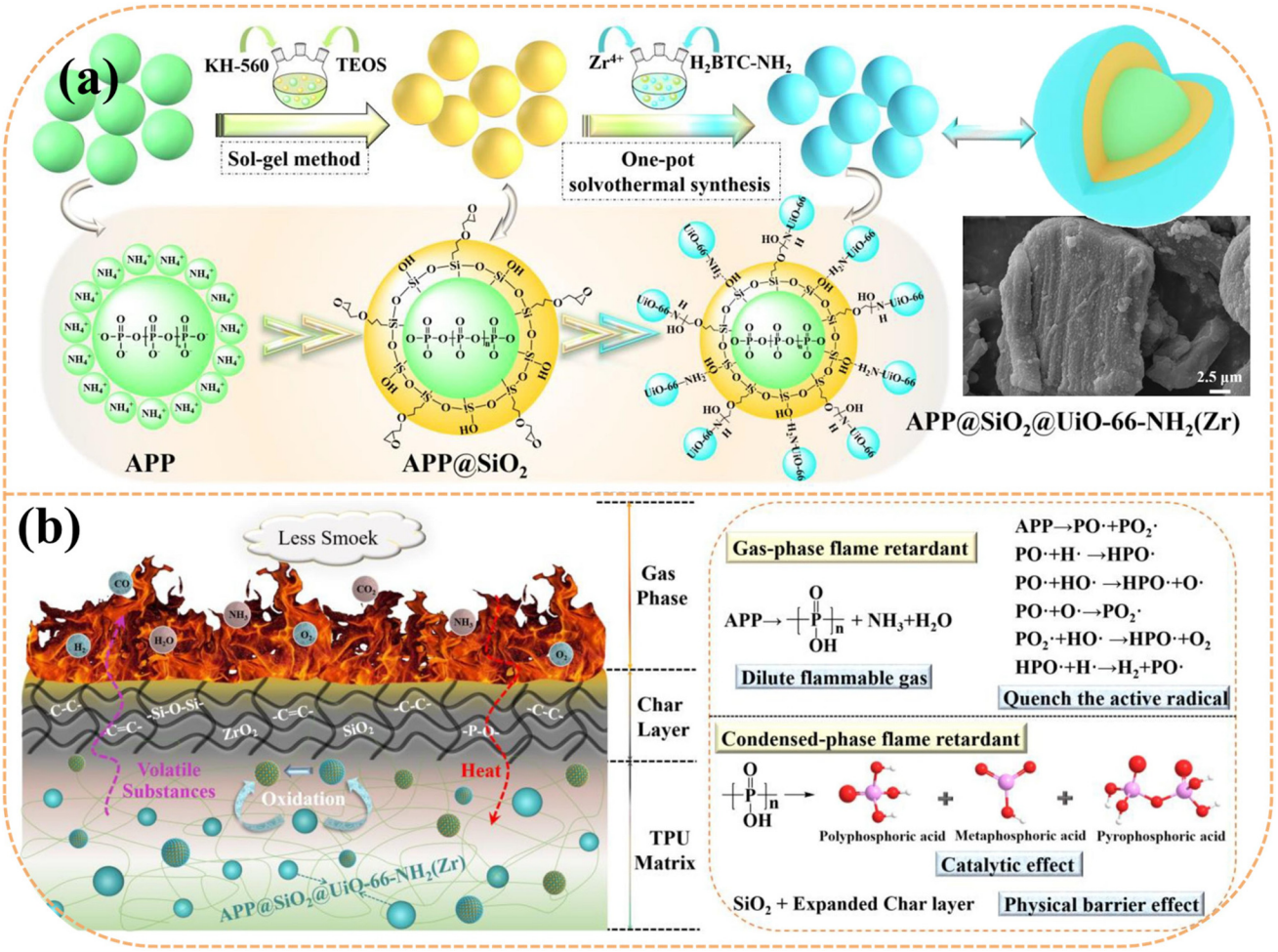

Fig. 5 (a) Schematic of the production route of APP@SiO_2@UiO-66-NH_2(Zr). (b) Flame retardant mechanism of the TPU composites. Reproduced with permission from ref. 64, copyright reserved Elsevier 2023.

(MWCNTs), and GO to enhance the flame retardant and smoke suppression properties of TPU. The TPU composite with 2 wt% GO@NH_2-UIO-66(Zr) reduced pHRR, THR, pSPR, and TSP by 74.6%, 35.0%, 64.3%, and 68.9%, respectively.

MOFs, as nanomaterials, tend to agglomerate, necessitating modification to improve their dispersion.[67] MXenes, 2D nanomaterials, offer excellent thermal stability, mechanical properties, and flame retardancy, but tend to restack.[68–70] As a modifier, MOF materials containing both organic and inorganic components is easy to establish close contact with MXenes and prevent restacking of layers. The synergy between MOFs and MXenes enhances MOF dispersion and improves MXenes' thermal stability, making it an effective strategy. Wan *et al.*[71] prepared 3D flower-like Ni-MOFs on layered MXene ($Ti_3C_2T_x$) *via* a solvothermal method (Fig. 6(a)) and studied their flame-retardant application in TPU. The composite with 2 wt% MOF@$Ti_3C_2T_x$ showed reductions in pHRR, THR, pSPR, TSP, TCOP, and TCO_2P by 19.5%, 3.3%, 35.3%, 22.9%, 25.4%, and 13.3%, respectively. The flame retardant mechanism (Fig. 6(b)) shows that Ni-MOF@$Ti_3C_2T_x$ employs both gas-phase and condensed-phase strategies, with the latter being dominant. This effect is mainly due to the catalytic and char-forming actions of Ni-MOF and $Ti_3C_2T_x$. The high-quality carbon layer acts as a physical barrier for heat and toxic gases transmission, enhancing flame retardancy. Shi *et al.*[72] synthesized a Co-MOF@MXene hybrid flame retardant through a solvothermal method, as shown in Fig. 6(c), and integrated it into TPU. The MXene modification effectively prevented Co-MOF aggregation, which is vital for enhancing its compatibility and dispersion within the TPU matrix. The composite with 2 wt% Co-MOF@MXene demonstrated reductions in pHRR, THR, pSPR, TSP, TCOP, and TCO_2P by 28.3%, 14.5%, 58.8%, 47.5%, 57.7%, and 35.9%, respectively, compared to pure TPU. As depicted in Fig. 6(d), the catalytic carbonization and physical barrier effects of Co-MOF@MXene contributed to a more cohesive and complete char layer, thereby significantly enhancing flame retardant efficiency. Bi *et al.*[73] utilized the dimension mismatch and collaborative stripping of 0D–1D–2D materials to incorporate SiC and ZIF-67 into MXene, effectively converting multilayered MXene into a single layer. Subsequently, polyaniline (PANI) was applied to the surface of MXene@SiC@ZIF, resulting in the functionalized nanohybrid

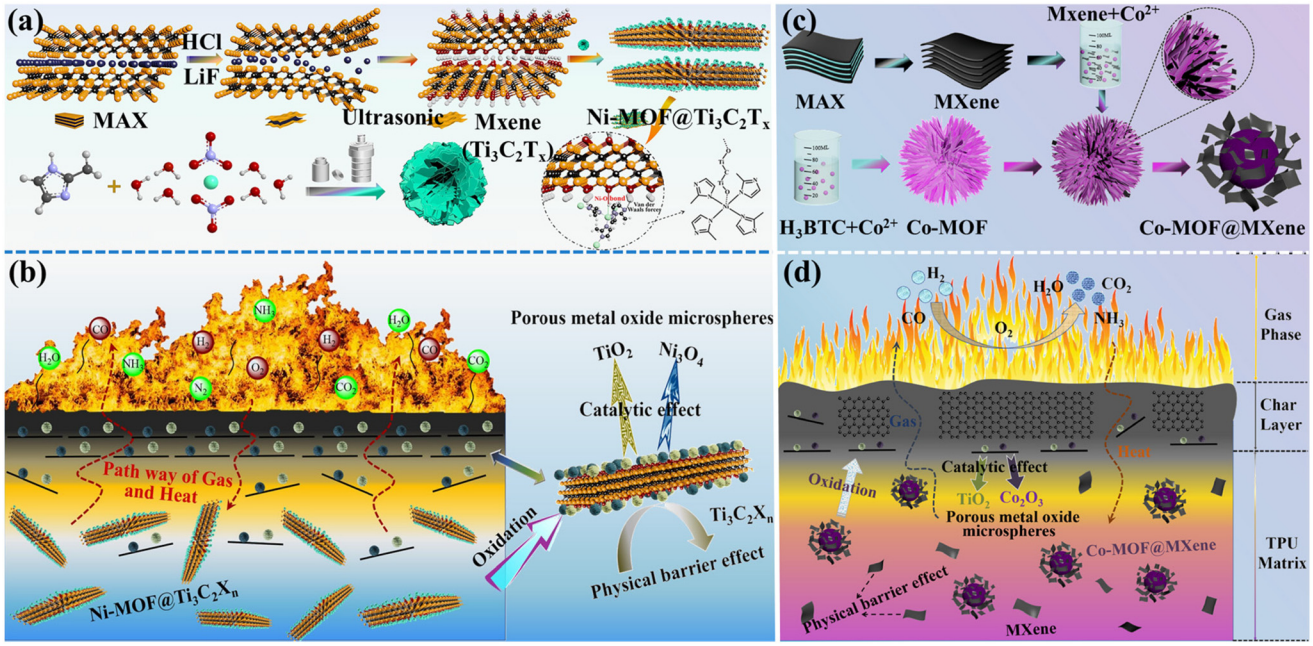

Fig. 6 (a) Schematic synthesis route of Ni-MOF@$Ti_3C_2T_x$ hybrids; (b) flame retardant mechanism of TPU composites. Reproduced with permission from ref. 71, copyright reserved Elsevier 2022. (c) Schematic synthesis route of Co-MOF@MXene hybrids. (d) Flame retardant mechanism of TPU composites. Reproduced with permission from ref. 72, copyright reserved Elsevier 2022.

material MXene@SiC@PANI, as shown in Fig. 7(a). This approach aimed to improve compatibility between the filler and polymer, and to enhance TPU's thermal conductivity, flame retardancy, and antibacterial properties. This material can be used in building materials, medical equipment, automobile interiors, electronic equipment, *etc*. The experimental results showed that the surface temperature of TPU composites with 5 wt% MXene@SiC@PANI increased from 33.4 °C to 59.8 °C within 10 s, reaching 95.0 °C within 60 s (Fig. 7(b)), confirming its superior heat absorption and transfer properties. Furthermore, the TPU composite demonstrated antibacterial efficiencies of 69.6% against *Escherichia coli* and 88.9% against *Staphylococcus aureus*. Compared to pure TPU, the pHRR, THR, pSPR, TSP, pCOP, and pCO_2P decreased by 71.4%, 34.6%, 72.8%, 49.1%, 72.3%, and 78.8%, respectively. The potential mechanisms for antibacterial and flame retardant actions are illustrated in Fig. 7(c). MXene nanosheets inflict direct physical damage on bacterial membranes through their sharp edges, causing the release of bacterial contents and ultimately leading to bacterial death. The multidimensional mixed-layer structure of the flame retardant actively contributes to barrier effects, metal catalysis, dilution of combustible gases, and carbonization. Wan *et al.*[74] employed polyethyleneimine (PEI), ZIF-67, MXene, and APP as raw materials to modify the surface of APP *via* a straightforward assembly strategy, successfully synthesizing a novel multilayer nanomaterial (APP-PEI@MXene@ZIF-67). The TPU/20% APP-PEI@MXene@ZIF-67-2BL composite exhibited reductions in pHRR, THR, pSPR, TSP, pCOP, and pCO_2P by 72.75%, 87.25%, 59.58%, 85.97%, 29.1%, and 74.5%, respectively, compared to pure TPU. To clearly compare the performance of MOF flame retardants reported in the literature, Table 1 presents the combustion performance of all TPU composite flame retardant materials.

3.3 Polyurethane foam

PUF can be produced during the PU preparation process by adding blowing agents (such as water, imines, Freon, *etc*.). The principle is based on the reaction between the blowing agent and isocyanate, which produces CO_2 or other gases, leading to the formation of numerous tiny bubbles within the material and resulting in a foam structure.[75] PUF can be categorized into RPUF and FPUF. The differences in hardness are mainly attributed to their degree of cross-linking and the content of soft/hard segments. RPUF has a higher cross-linking density and a greater proportion of hard segments, which form microcrystalline structures within the foam, further enhancing the material's rigidity and hardness.[76] FPUF, on the other hand, exhibits the opposite characteristics. Tables 2 and 3 summarize the flame retardancy data from research papers on MOF-based flame retardant RPUF and FPUF, respectively.

3.3.1 Rigid polyurethane foam (RPUF). RPUF is extensively utilized in packaging materials, as well as thermal insulation and soundproofing materials.[77] However, its aliphatic segments and porous structure render RPUF highly flammable, thus limiting its application scope. Cheng *et al.*[78] synthesized three types of ZIFs (ZIF-7, ZIF-8, and ZIF-11) as flame retardants, incorporating them into RPUF at a loading of 12 wt%. The results indicated that the maximum compressive strength of ZIFs/RPUF increased from 7.96 MPa to 8.9 MPa compared to

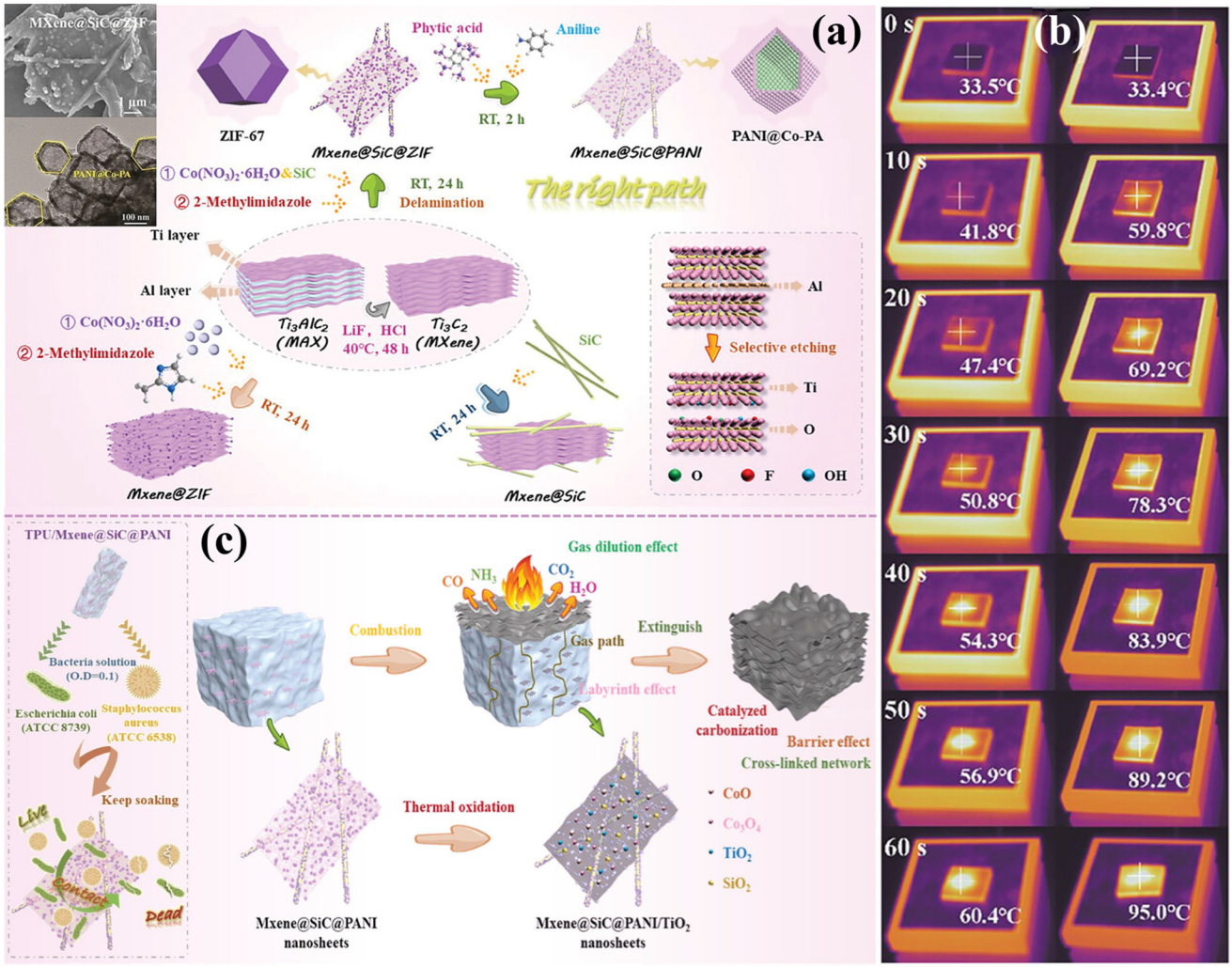

Fig. 7 (a) Schematic of the synthesis of MXene@SiC@PANI; (b) infrared thermography of TPU/MXene@SiC@PANI composites during heating; (c) antimicrobial process and flame-retardant mechanism of composite TPU. Reproduced with permission from ref. 73, copyright reserved Wiley 2024.

Table 2 Flame retardant properties of MOF composite RPUF compared to pure RPUF

Type of FRs	Loading (wt%)	LOI/*T* (%/mm)	UL-94/*T* (mm)	Main flame-retardant results/*T* (mm)	Ref.
ZIF-7	12.0	—	—	19.2%, 19.6%, 15.2% and 8.3% reduction in pHRR, THR, pSPR and TSP (heat flux of 50 kW m^{-2})	78
ZIF-8	12.0	—	—	33.9%, 29.3%, 32.1% and 23.9% reduction in pHRR, THR, pSPR and TSP (heat flux of 50 kW m^{-2})	
ZIF-11	12.0	—	—	21.3%, 19.8%, 15.2% and 8.3% reduction in pHRR, THR, pSPR and TSP (heat flux of 50 kW m^{-2})	
ZMD	10.0	25.4/10.0	—	50.1%, 61.8%, 70.6% and 76.1% reduction in pHRR, THR, pSPR and TSP/25.0 (heat flux of 50 kW m^{-2})	79
N-ZIF-8	15.0	—	—	35.73% and 39.17% reduction in pHRR and THR/10.0 (heat flux of 35 kW m^{-2})	80
TBPBP/C-MOF/MWCNTs	16.4/3.6	46.35	V-0	47.54%, 47.97%, 38.54%, 50.46%, 55.56%, 16.48%, 41.38% and 43.37% reduction in pHRR, THR, pSPR, TSP, pCOP, pCO_2P, TCOP and TCO_2P	85
APP@PDA-ZIF	10.0	25.6/5.0	V-0	38.6%, 45.9%, 19.2%, 53.4% and 38.1% reduction in pHRR, THR, pSPR, TSP and pCOP/10.0 (heat flux of 35 kW m^{-2})	86

T represents thickness. If *T* and heat flux are not indicated, the reference does not provide data.

Table 3 Flame retardant properties of MOF composite FPUF compared to pure FPUF

Type of FRs	Loading (wt%)	LOI/*T* (%/mm)	Main flame-retardant results/*T* (mm)	Ref.
LFPN@PDA@MOF	—	—	15.1%, 9.5%, 17.0%, 7.7%, 38.1%, 18.3%, −1.2% and −64.1% reduction in pHRR, THR, pSPR, TSP, pCOP, pCO_2P, TCOP and TCO_2P/3.0 (heat flux of 35 kW m^{-2})	88
ZIF-8	—	18.8	50.6%, 16.5%, 35.5% and 16.0% reduction in pHRR, THR, pSPR and TSP	90
Cu (BDC)-NGPs	—	24.46	—	91
MOFs-NH2	—	21.5	64.3%, 60.0%, 33.7%, 15.2%, 35.2% and 29.5% reduction in pHRR, THR, pSPR, TSP, TCOP and TCO_2P/30.0 (heat flux of 35 kW m^{-2})	92
BN@MOF-LDH@APTES	5.0	—	8.5%, 15.7%, 6.8% and 15.8% reduction in pHRR, THR, pSPR and TSP/25.0	93
MOF-LDH@HDTMS	—	—	30.3%, 20.6% and 29.9% reduction in pHRR, pSPR and pCOP (heat flux of 35 kW m^{-2})	94

T represents thickness. If *T* and heat flux are not indicated, the reference does not provide data.

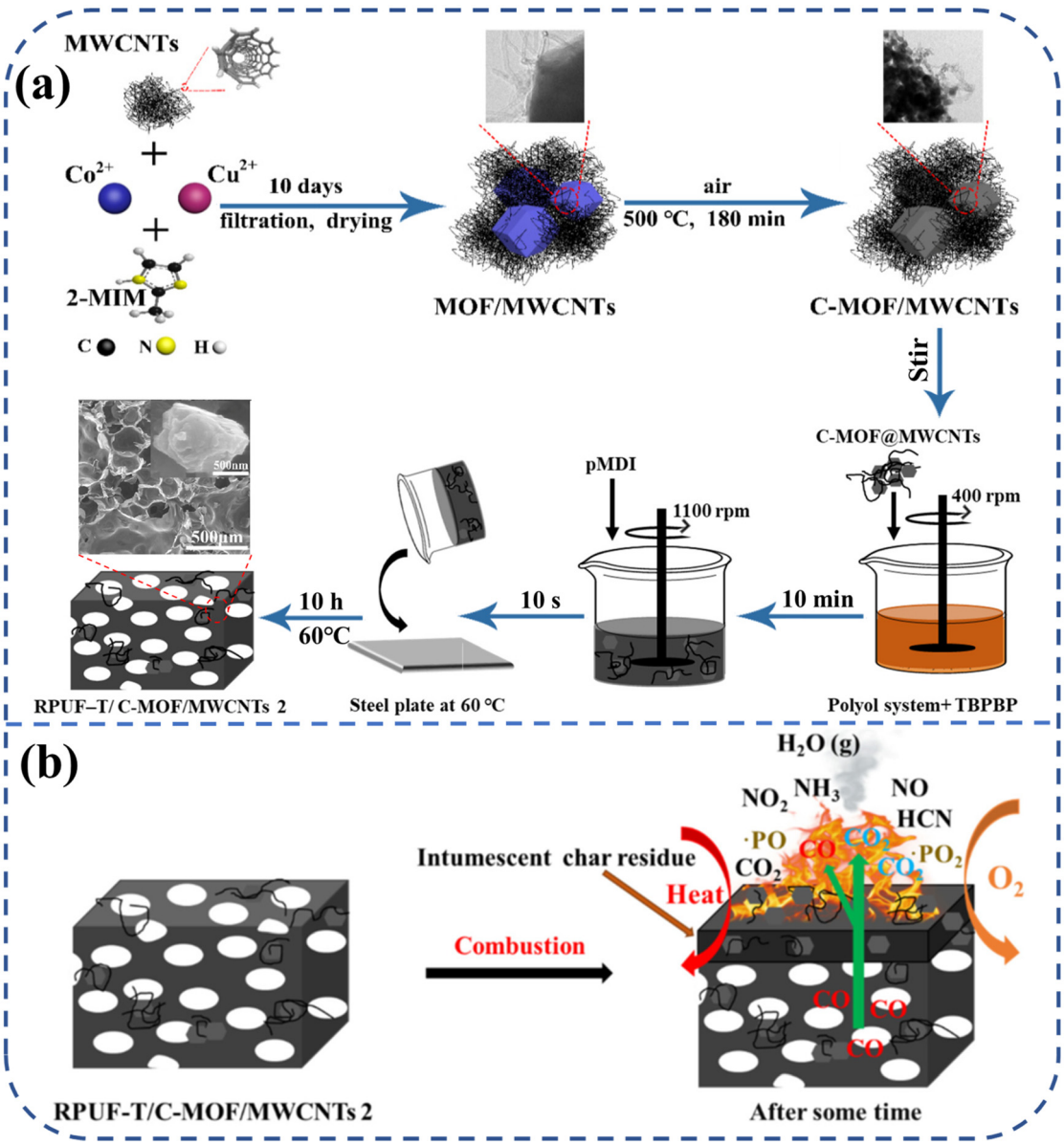

Fig. 8 (a) Schematic diagram of preparation and (b) flame retardant mechanism of bio-based RPUF-T/C-MOF/MWCNTs. Free copyright reserved MDPI 2022.

pure RPUF. The flame retardant properties of ZIF-7/RPUF, ZIF-8/RPUF, and ZIF-11/RPUF are detailed in Table 2. Among these, ZIF-8 demonstrated the most effective flame-retardant performance, indicating that further research into novel MOFs such as ZIF-8 could significantly advance the development of flame-retardant and smoke-suppressing RPUF composites. Xu *et al.*[79] developed a core–shell structure of ZIF-8@melamine (MA) and successfully synthesized a Si–N–Zn ternary composite material (ZMD) by modifying ZIF-8@MA with diatomite. The results revealed that the addition of 10 wt% ZMD to RPUF resulted in decreases of 50.1%, 61.8%, 70.6%, and 76.1% in pHRR, THR, pSPR, and TSP, respectively. Moreover, the LOI

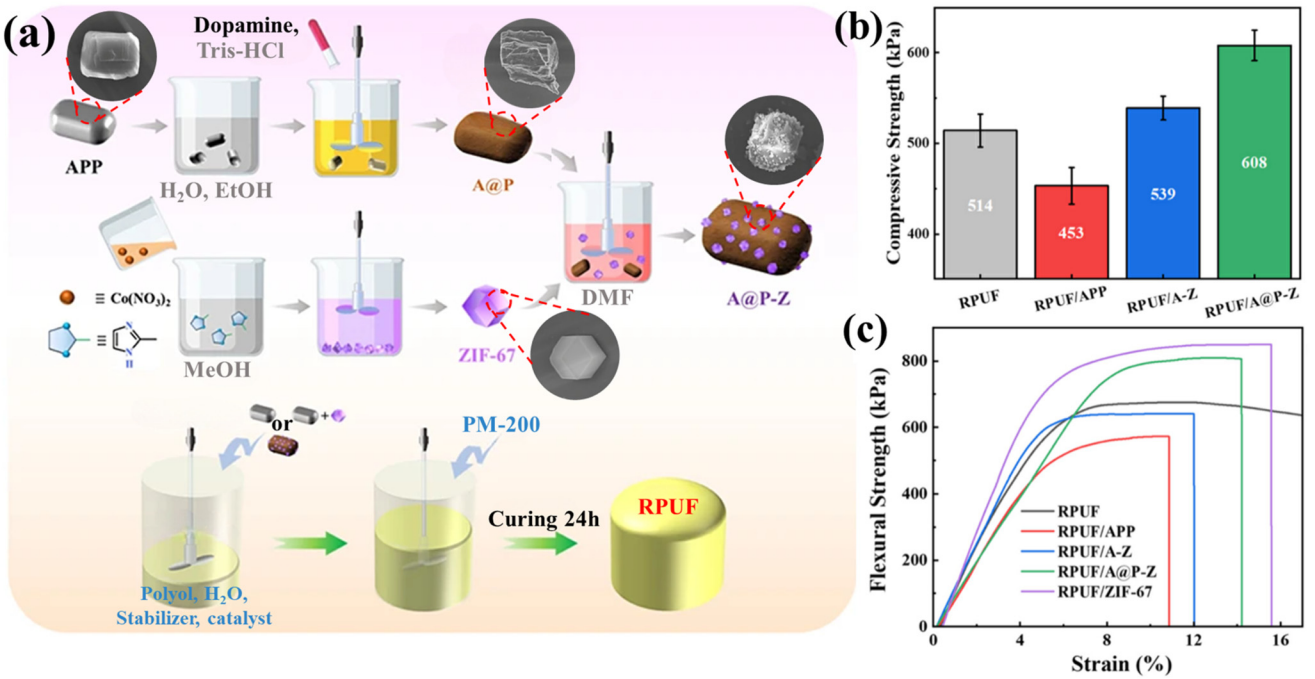

Fig. 9 (a) Flow chart for the preparation of A@P-Z and RPUF composites; (b) 10% compressive strength and (c) flexural strength of RPUF and its composites. Reproduced with permission from ref. 86, copyright reserved Wiley 2018.

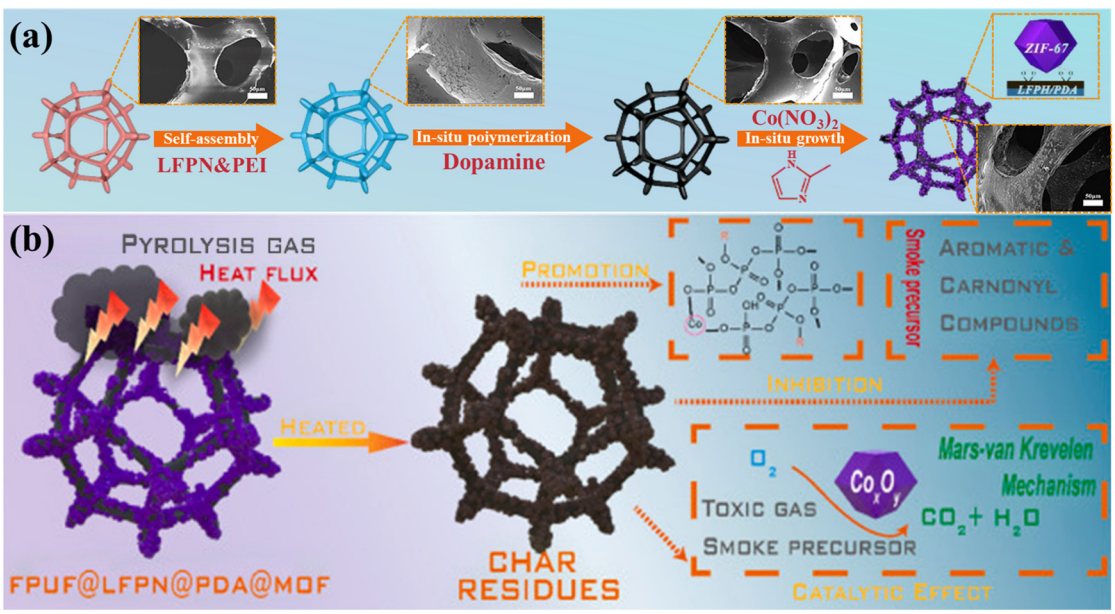

Fig. 10 (a) Preparation process and (b) flame retardant mechanism of FPUF@LFPN@PDA@MOF. Reproduced with permission from ref. 88, copyright reserved Elsevier 2024.

value of RPUF increased from 19.4% to 25.4%. Liang *et al.*[80] successfully synthesized N-rich ZIF-8 (N-ZIF-8), which exhibited enhanced flame-retardant properties. The N content in N-ZIF-8 was increased by 79.17%. The results indicated that, compared to pure RPUF, the composite containing 15 wt% N-ZIF-8 exhibited reductions in pHRR and THR by 35.7% and 39.1%, respectively.

In light of environmental protection and sustainability concerns, advancing bio-based PU is crucial.[81,82] Bio-based RPUF commands a significant market share due to its high specific strength, low thermal conductivity, light weight, and cost-effectiveness, making it extensively used as an insulation material across various sectors.[83,84] Bo *et al.*[85] initially mixed Cu ion-partially substituted ZIF-67 with MWCNTs, followed by calcination in air to produce C-MOF/MWCNTs. The C-MOF/MWCNTs were integrated into renewable bio-based RPUF containing a P–N reactive flame retardant (TBPBP), as depicted in Fig. 8(a). The findings revealed that RPUF-T/C-MOF/MWCNTs outperformed all comparison groups. Specifically, compared to pure RPUF, the compressive strength, LOI, and char residue for RPUF-T/C-MOF/MWCNTs increased by 105.93%, 46.35%, and 347.32%, respectively. Concurrently, the pHRR, THR, pSPR, TSP, pCOP, and pCO_2P decreased by 47.54%, 47.97%, 38.54%, 50.46%, 55.56%, and 16.48%, respectively. RPUF-T/C-MOF/MWCNTs utilized a dual flame-retardant strategy, integrating both condensed-phase and gas-phase mechanisms, as showed in Fig. 8(b). This material offers valuable insights into the development of safe and environmentally friendly RPUF insulation materials for the construction industry.

As shown in Fig. 9(a), Liu *et al.*[86] combined APP, PDA, and ZIF-67 into a ternary inorganic–organic hybrid flame retardant (A@P-Z) by using biomass polydopamine (PDA) as an interfacial medium. The mechanical properties of the RPUF composite were significantly enhanced by the hybrid flame retardant; RPUF/A@P-Z achieved a maximum flexural strength of 815 kPa and a flexural strain limit of 14.2%, both of which were greater than those of pure RPUF (see Fig. 9(b and c)). Relative to pure RPUF, the pHRR, THR, pSPR, TSP, and pCOP of RPUF/A@P-Z were reduced by 38.6%, 45.9%, 19.2%, 53.4%, and 38.1%, respectively, while the LOI increased from 19.7% to 25.6%, achieving UL-94 V-0 rating.

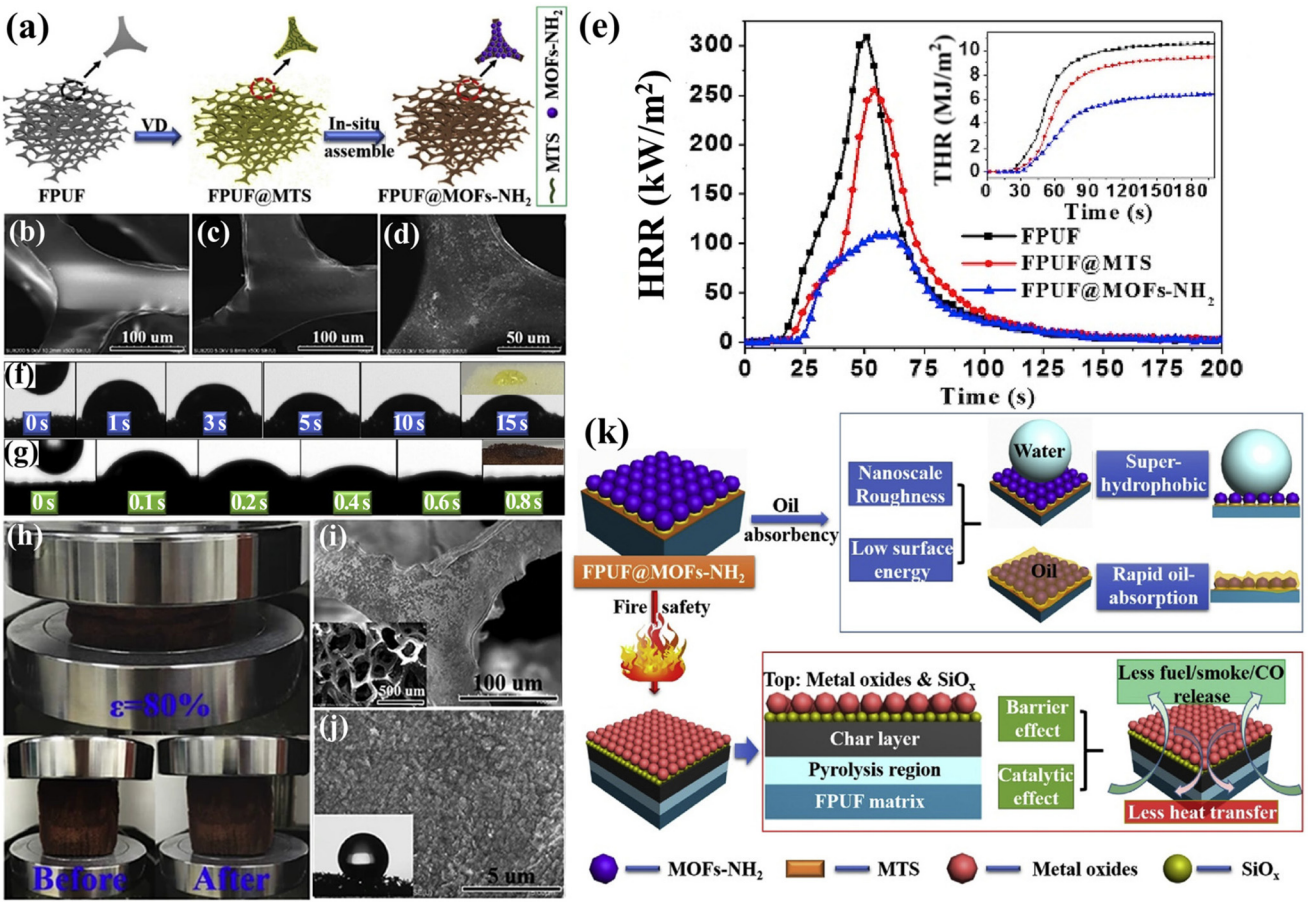

Fig. 11 (a) Schematic diagram of FPUF@MOFs-NH_2 sponge preparation process; (b) SEM images of pure FPUF, (c) FPUF@MTS, and (d) FPUF@MOFs-NH_2; (e) heat release curves of FPUF and its composites; absorption process of soybean oil by (f) pure FPUF and (g) FPUF composite sponge; (h) digital images of FPUF composite sponge compression test; (i and j) SEM images of FPUF composite sponge after 1000 compression tests at different magnifications. (k) Oil absorption and flame retardant mechanism diagram of FPUF composite sponge. Reproduced with permission from ref. 92, copyright reserved Elsevier 2019.

3.3.2 Flexible polyurethane foam (FPUF). FPUF is extensively utilized in orthopedic supports, automotive seats, and furniture upholstery because of its superior resilience, tensile strength, and low density.[87] Nevertheless, its chemical composition and porous structure make it highly flammable, and the toxic gases emitted during combustion present substantial safety hazards. The development of flame retardant FPUF with adsorption function is currently a hot research trend. Geng *et al.*[88] successfully developed an efficient flame retardant (LFPN@PDA@MOF) with smoke suppression and toxicity reduction properties. By using PDA to facilitate the *in situ* growth of ZIF-67 and lignocellulose-based P–N flame retardants (LFPN), they aimed to enhance FPUF's flame retardancy (see Fig. 10(a)). Relative to pure FPUF, the pHRR, THR, pSPR, and TSP of FPUF@LFPN@PDA@MOF were reduced by 15.1%, 9.5%, 17.0%, and 7.7%, respectively. Similarly, toxic gases like CO and HCN also demonstrated downward trends. The smoke and toxicity reduction mechanism of FPUF@LFPN@PDA@MOF, as illustrated in Fig. 10(b), can be summarized as the "inhibition" of smoke precursors and the "catalysis" of toxic gases.

Spills of oil and toxic chemical solvents in industries such as petrochemicals and pharmaceuticals have led to significant ecological and environmental issues globally.[89] Furthermore, most spilled crude oil and organic solvents are highly flammable and explosive. Consequently, employing flame-retardant FPUF as a sponge to absorb organic solvents, thereby mitigating or even eliminating the potential risk of fires and explosions, presents a viable solution. Zhao *et al.*[90] successfully developed a ZIF-8-coated modified FPUF sponge material. The modified FPUF demonstrated excellent adsorption capacity and recyclability for various oils and organic solvents, with a maximum absorption capacity of up to 33 times its own weight. Additionally, the pHRR, THR, pSPR, and TSP values of ZIF-8-modified FPUF were reduced by 50.6%, 16.5%, 35.5%, and 16.0%, respectively. The LOI value of ZIF-8/FPUF increased from 17.2% (pure FPUF) to 18.8%. This flame-retardant oil-absorbing material represents a promising solution for addressing oil and chemical solvent spill incidents. Habibi *et al.*[91] modified FPUF sponges by incorporating a Cu-benzene dicarboxylic acid metal–organic framework (Cu (BDC) MOF) and nano graphite platelets (NGPs). The resulting PU-Cu(BDC)-

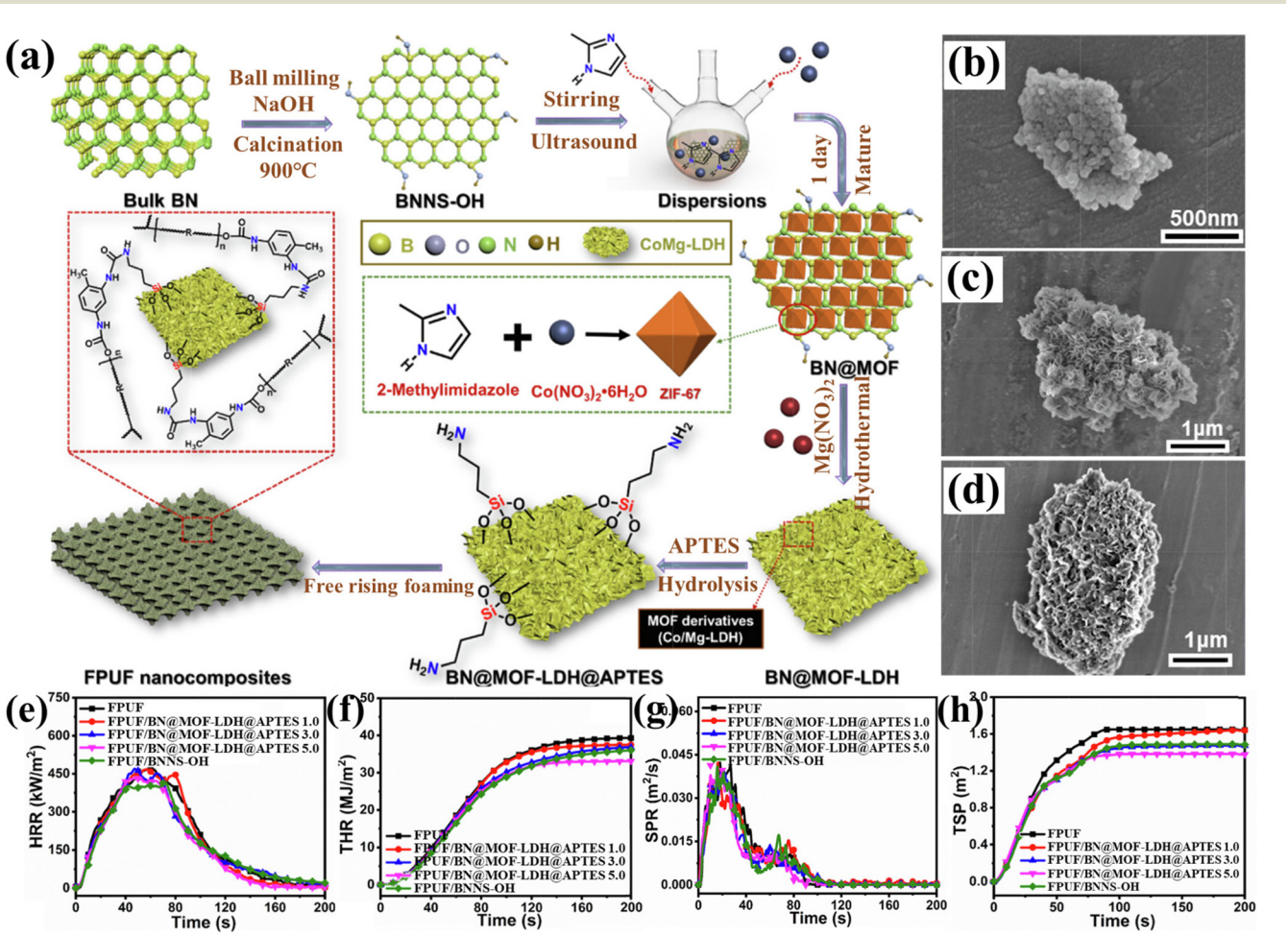

Fig. 12 (a) Preparation flow of BN@MOF-LDH@APTES nanohybrids; SEM images of (b) BN@MOF, (c) BN@MOF-LDH and (d) BN@MOF-LDH@APTES; (e) HRR, (f) THR, (g) SPR and (h) TSP curves of FPUF and its composites. Reproduced with permission from ref. 93, copyright reserved Elsevier 2022.

NGPs composite material exhibited exceptional superhydrophobicity, achieving 96% oil–water separation efficiency, and demonstrated self-extinguishing properties with an LOI value of 24.46%. Hou *et al.*[92] employed a vapor deposition method to modify FPUF with (3-Mercaptopropyl) trimethoxysilane (MTS), subsequently synthesizing nano-amino bimetallic metal–organic frameworks (MOFs-NH_2) *in situ* on the FPUF skeleton (see Fig. 11(a–d)). This process yielded FPUF@MOFs-NH_2 composite materials with outstanding flame retardancy and oil absorption properties. Compared to pure FPUF, the pHRR and THR of FPUF@MOFs-NH_2 was reduced by 64.3% and 60% (Fig. 11(e)). Fig. 11(f and g) illustrate the oil penetration process on the surface of PFUF and FPUF@MOFs-NH_2. FPUF composite sponge rapidly absorbed soybean oil in under 1 s, demonstrating its swift oil absorption capability. After 1000 compression tests at 80% strain, no significant structural damage was observed in the FPUF composite sponge (Fig. 11(h–j)), confirming its mechanical stability. A schematic diagram showing its oil absorption and flame retardancy mechanisms is presented in Fig. 11(k). The nano-sized MOFs-NH_2 contribute to the sponge's nanostructure, reducing surface free energy, and thereby enhancing oil absorption. The external heat source induces the thermal decomposition of MOFs-NH_2 and MTS into metal oxides and SiO_x, which suppresses heat transfer between the decomposition products and both the pyrolysis and combustion zones, while also catalyzing the conversion of organics and toxic gases into char residues.

Zhou *et al.*[93] utilized MOF-derived petal-like Co/Mg-double metal hydroxide (Co/Mg-LDH) and 3-aminopropyltriethoxysilane (APTES) to modify hydroxylated boron nitride (BNNS-OH), resulting in hydrophobic BN@MOF-LDH@APTES. The preparation process is illustrated in Fig. 12(a). The SEM images (Fig. 12(b–d)) depict the growth process of MOF-derived LDH and APTES. Tests showed that FPUF composites with 1 wt% BN@MOF-LDH@APTES exhibited excellent resilience and adsorption capacity, achieving a 71% increase in compressive strength, and could be reused without loss of oil absorption capability. Moreover, FPUF composites with 5 wt% BN@MOF-LDH@APTES demonstrated reductions in pHRR, THR, pSPR, and TSP by 8.5%, 15.7%, 6.8%, and 15.8%, respectively (see Fig. 12(e–g)). Inspired by desert beetles and lotus leaves, Piao *et al.*[94] developed a flame-retardant sponge for continuous oil–water separation (FPUF@MOF-LDH@HDTMS), as shown in Fig. 13(a), by *in situ* growth of ZIF-67-derived layered double hydroxide (MOF-LDH) on the surface of FPUF, followed by grafting with hexadecyltrimethoxysilane (HDTMS). As shown in Fig. 13(b and c), water droplets (blue) remained spherical on the sponge surface, while oil droplets (red) were rapidly absorbed by FPUF@MOF-LDH@HDTMS, achieving an oil–water separation efficiency of 99.1%, thereby demonstrating its strong hydrophobic/oleophilic properties. Compared to FPUF, pHRR, pSPR, and pCOP of FPUF@MOF-LDH@HDTMS decreased by 30.3%, 20.6%, and 29.9%, respectively. The flame-retardant mecha-

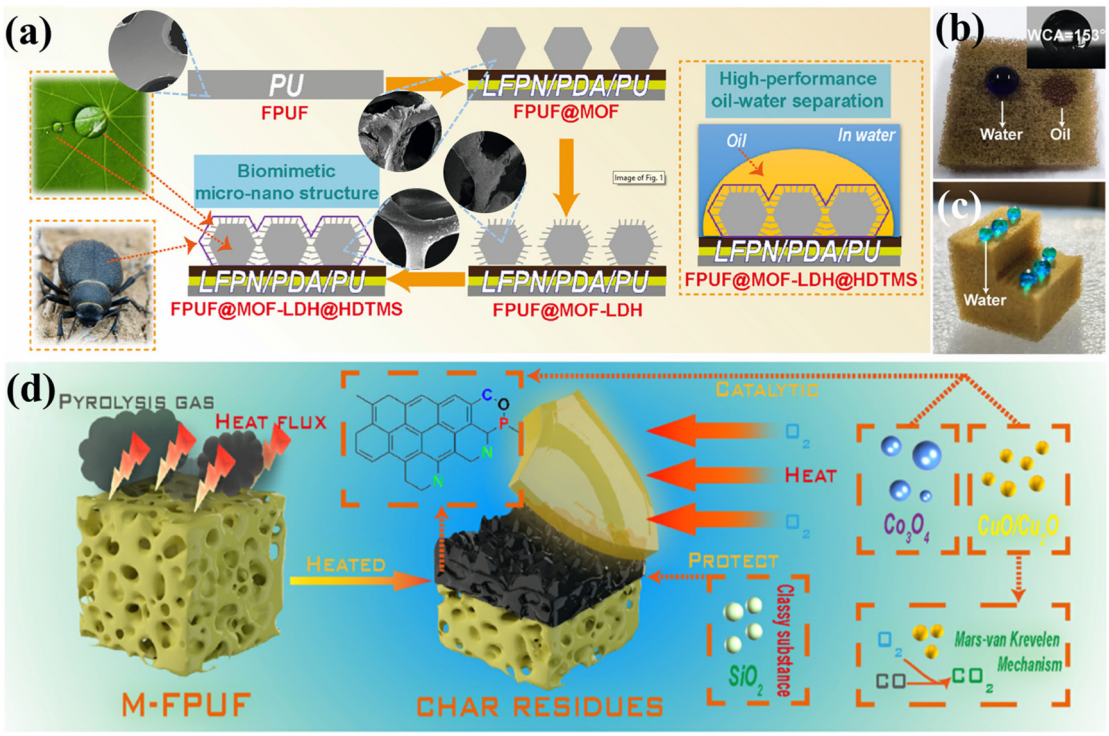

Fig. 13 (a) Schematic of FPUF@MOF-LDH@HDTMS bionic structure and oil–water separation mechanism; (b and c) wettability of FPUF@MOF-LDH@HDTMS; (d) flame retardant mechanism of FPUF composite. Reproduced with permission from ref. 94, copyright reserved Elsevier 2023.

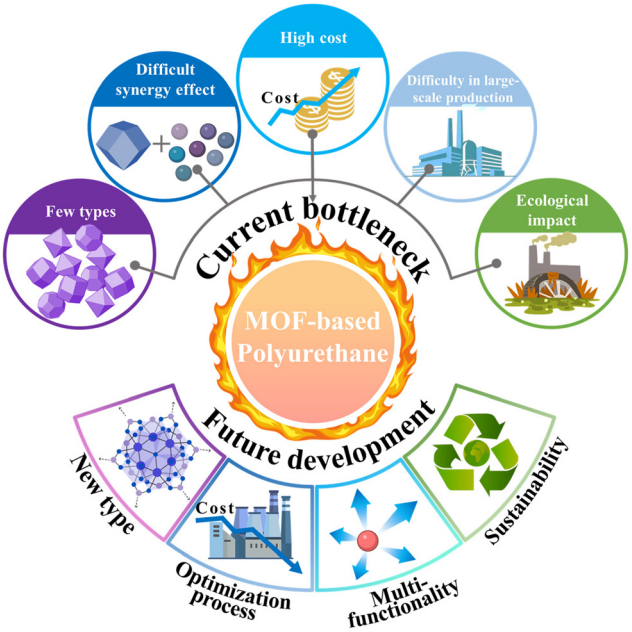

Fig. 14 The main bottlenecks and future development directions of MOF-based PU flame retardant materials.

nism of FPUF composite is depicted in Fig. 13(d). During combustion, MOF-LDH@HDTMS generates oxides (such as Cu_2O/CuO, Co_3O_4, and SiO_2), which form a dense, continuous char layer that inhibits the ingress of O_2 and heat, as well as the release of flammable gases.

4. Conclusions and prospects

MOF-based materials, as novel flame retardants, have demonstrated significant potential in PU applications. These substances perform exceptionally well in reducing toxicity and smoke while also significantly improving PU's flame retardancy. Current research indicates that combining MOFs with other nanomaterials (such as MXene, EG, and GO) can further enhance their flame retardant effects in PU. Overall, the introduction of MOF-based flame retardants offers a new approach to traditional PU flame retardant systems, carrying important scientific significance and application prospects.

Fig. 14 summarizes the main bottlenecks and future directions in the research field of MOF-based PU flame-retardant materials. The current challenges and limitations include:

(1) The MOFs currently used for flame-retardant PU are mainly derived from ZIF-67 and ZIF-8, with relatively few studies on other types of MOFs. This limits their broader application across different PU materials. Different MOFs possess varying structures and properties, but existing research has predominantly focused on only a few types, thus not fully leveraging the diversity of MOF materials.

(2) Although MOFs perform excellently in enhancing PU flame retardancy, their flame-retardant effect often requires synergistic action with other flame retardants to achieve optimal results. While this synergistic effect improves flame retardant efficiency, it also increases the complexity of designing the flame retardant system and may impact the final material properties.

(3) MOFs exhibit promising flame retardant properties, but the complexity of synthesizing MOF-based flame retardants and their high production costs hinder their widespread commercial adoption. Cost-effective synthesis methods and cheaper raw materials need to be developed to make MOF-based flame retardants economically viable on a large scale.

(4) While current synthesis methods are effective for laboratory-scale research, scaling up for industrial production often presents challenges. Efficient and high-yield methods that maintain the quality and performance of MOFs are crucial for industrial applicability.

(5) Concerns concerning MOFs' long-term environmental effects, including biodegradability and the environmental costs of large-scale production, persist despite the fact that they are generally composed of non-toxic metals and organic linkers.

Further design and synthesis of novel MOF materials with specific functions is necessary to increase the application of MOFs in flame-retardant PU. Future research should focus on exploring different combinations of metal centers and organic ligands to develop a broader range of MOF materials. To achieve the industrial application of MOF-based flame retardants, simplifying their preparation processes and reducing production costs will be key. By optimizing synthetic routes and process parameters, it is possible to improve the preparation efficiency of MOF materials and reduce material costs. Additionally, attention should be paid to optimizing other properties of MOF-based flame retardants, such as mechanical properties, thermal stability, and processing performance, while maintaining or enhancing PU's flame retardancy to meet practical application requirements. Furthermore, developing environmentally friendly MOF-based flame retardants is an important direction for future research. MOF materials based on renewable resources and green synthesis methods will have broader application prospects.

Data availability

No data was used for the research described in the article.

Conflicts of interest

There are no conflicts to declare.

Acknowledgements

The National Natural Science Foundation of China (No. 22375023, 22005029), the Natural Science Foundation of Chongqing (CSTB2024NSCQ-MSX0452), and the Hebei Natural

Science Foundation (E2024105006) provided funding for this work.

References

1 S. Lu, Y. Feng, P. Zhang, W. Hong, Y. Chen, H. Fan, D. Yu and X. Chen, *Polymers*, 2021, **13**, 1730.
2 F. Xie, T. Zhang, P. Bryant, V. Kurusingal, J. M. Colwell and B. Laycock, *Prog. Polym. Sci.*, 2019, **90**, 211–268.
3 X. Jin, J. Dong, X. Guo, M. Ding, R. Bao and Y. Luo, *Polym. Int.*, 2022, **71**, 1384–1392.
4 A. Das and P. Mahanwar, *Adv. Ind. Eng. Polym. Res.*, 2020, **3**, 93–101.
5 J. O. Akindoyo, M. D. H. Beg, S. Ghazali, M. R. Islam, N. Jeyaratnam and A. R. Yuvaraj, *RSC Adv.*, 2016, **6**, 114453–114482.
6 Y. Mo, X. Huang and C. Hu, *Polymers*, 2024, **16**, 2155.
7 H. Nabipour, X. Wang, L. Song and Y. Hu, *Composites, Part A*, 2020, **139**, 106113.
8 J. Chen, Y. Wang, Y. Yu, J. Wang, J. Liu, H. Ihara and H. Qiu, *Exploration*, 2023, **3**, 20220144.
9 Y.-T. Pan, Z. Zhang and R. Yang, *Composites, Part B*, 2020, **199**, 108265.
10 X. Song, B. Hou, Z. Han, Y.-T. Pan, Z. Geng, L. H Ibarra and R. Yang, *Chem. Eng. J.*, 2023, **470**, 144278.
11 K. Song, Y.-T. Pan, J. Zhang, P. Song, J. He, D.-Y. Wang and R. Yang, *Chem. Eng. J.*, 2023, **468**, 143653.
12 Y. Sun, Z. Xue, Q. Liu, Y. Jia, Y. Li, K. Liu, Y. Lin, M. Liu, G. Li and C. Y. Su, *Nat. Commun.*, 2021, **12**, 1369.
13 W. P. Lustig, S. Mukherjee, N. D. Rudd, A. V. Desai, J. Li and S. K. Ghosh, *Chem. Soc. Rev.*, 2017, **46**, 3242–3285.
14 G. L. Yang, X. L. Jiang, H. Xu and B. Zhao, *Small*, 2021, **17**, 2005327.
15 H. D. Lawson, S. P. Walton and C. Chan, *ACS Appl. Mater. Interfaces*, 2021, **13**, 7004–7020.
16 B. Hou, K. Song, Z. Ur Rehman, T. Song, T. Lin, W. Zhang, Y.-T. Pan and R. Yang, *ACS Appl. Mater. Interfaces*, 2022, **14**, 14805–14816.
17 H. Q. Yan, J. W. Jiang, T. Zhu, Z. H. Guo, S. Y. Ran, J. Li, T. Sai and Z. P. Fang, *ACS Appl. Polym. Mater.*, 2024, **6**, 4256–4266.
18 J. Cao, Y.-T. Pan, H. Vahabi, J. I. Song, P. Song, D.-Y. Wang and R. Yang, *Mater. Today Chem.*, 2024, **37**, 102015.
19 S. Qiu, Z. Cheng, Y. Li, Y. Hu and L. Zhang, *ACS Appl. Nano Mater.*, 2024, **7**, 14727–14736.
20 R. Lian, H. Guan, Y. Zhang, M. Ou, Y. Jiang, L. Liu, C. Jiao and X. Chen, *Polym. Degrad. Stab.*, 2023, **217**, 110534.
21 S. Yu, C. Cheng, K. Li, J. Wang, Z. Wang, H. Zhou, W. Wang, Y. Zhang and Y. Quan, *Chem. Eng. J.*, 2023, **465**, 143039.
22 P. Lyu, Y. Hou, J. Hu, Y. Liu, L. Zhao, C. Feng, Y. Ma, Q. Wang, R. Zhang, W. Huang and M. Ma, *Polymers*, 2022, **14**, 5279.
23 H. Zhao, B. Yuan, Y. Zhan, F. Yang, J. Zhou, C. Qi, C. Lei and Y. Li, *Composites, Part A*, 2022, **159**, 107003.
24 Y. Hou, W. Hu, Z. Gui and Y. Hu, *Ind. Eng. Chem. Res.*, 2017, **56**, 2036–2045.
25 K. Song, H. Zhang, Y.-T. Pan, Z. Ur Rehman, J. He, D.-Y. Wang and R. Yang, *J. Colloid Interface Sci.*, 2023, **643**, 489–501.
26 Z. Han, X. Song, Z. Chen, Y.-T. Pan, X. Lai, D.-Y. Wang and R. Yang, *Sustainable Mater. Technol.*, 2024, **41**, e01024.
27 Z. Han, W. Zhang, X. Song, H. Vahabi, Y.-T. Pan, W. Zhang and R. Yang, *Chem. Eng. J.*, 2023, **474**, 145682.
28 K. Song, X. Bi, C. Yu, Y.-T. Pan, H. Vahabi, V. Realinho, J. He and R. Yang, *ACS Appl. Mater. Interfaces*, 2024, **16**, 7617–7630.
29 X. Bi, Z. Zhang, K. Song, X. Zhang, Y.-T. Pan, H. Qu, H. Vahabi, J. He and R. Yang, *Composites, Part A*, 2024, **184**, 108283.
30 X. Bi, K. Song, Y.-T. Pan, C. Barreneche, H. Vahabi, J. He and R. Yang, *Small*, 2024, **20**, 2307492.
31 X. Bi, X. Cheng, Z. Zhang, Y. Huang, Y.-T. Pan, J. Guan, M. Ardanuy and R. Yang, *Next Mater.*, 2024, **3**, 100143.
32 W. Meng, H. Wu, X. Bi, Z. Huo, J. Wu, Y. Jiao, J. Xu, M. Wang and H. Qu, *Microporous Mesoporous Mater.*, 2021, **314**, 110885.
33 X. G. Wang, P. Qi, S. J. Zhang, S. L. Jiang, Y. C. Li, J. Sun, B. Fei, X. Y. Gu and S. Zhang, *Mater. Today Chem.*, 2023, **30**, 101550.
34 B. Hou, Y.-T. Pan and P. Song, *Microstructures*, 2023, **3**, 2023039.
35 X. Bi, K. Song, H. Zhang, Y.-T. Pan, J. He, D.-Y. Wang and R. Yang, *Chem. Eng. J.*, 2024, **482**, 148997.
36 H. Yang, Y. Qin, D. Liang, X. Lu and X. Gu, *J. Therm. Anal. Calorim.*, 2023, **148**, 12845–12857.
37 J. Cao, B. Zhang, J. Zhang, R. Duan, Y. Jiao, H. Qu and J. Xu, *Mater. Lett.*, 2024, **361**, 136062.
38 B. Hou, W. Zhang, H. Lu, K. Song, Z. Geng, X. Ye, Y.-T. Pan, W. Zhang and R. Yang, *ACS Appl. Mater. Interfaces*, 2022, **14**, 49326–49337.
39 K. Song, X. Li, Y.-T. Pan, B. Hou, Z. U. Rehman, J. He and R. Yang, *Polym. Degrad. Stab.*, 2023, **211**, 110318.
40 K. Song, Y.-T. Pan, J. He and R. Yang, *Ind. Chem. Mater.*, 2024, DOI: **10.1039/d3im00110e**.
41 X. Song, Q. Li, Z. Han, B. Hou, Y.-T. Pan, Z. Geng, J. Zhang, L. H Ibarra and R. Yang, *J. Colloid Interface Sci.*, 2024, **667**, 223–236.
42 Y.-T. Pan, Y. Yuan, D.-Y. Wang and R. Yang, *Chin. J. Chem.*, 2020, **38**, 1870–1896.
43 M. Woellner, S. Hausdorf, N. Klein, P. Mueller, M. W. Smith and S. Kaskel, *Adv. Mater.*, 2018, **30**, 1704679.
44 Y. Li, M. Zhou, R. Wang, H. Han, Z. Huang and J. Wang, *Eur. Polym. J.*, 2024, **214**, 113159.
45 D. K. Chattopadhyay and D. C. Webster, *Prog. Polym. Sci.*, 2009, **34**, 1068–1133.
46 B. Xu, W. Xu, Y. Liu, R. Chen, W. Li, Y. Wu and Z. Yang, *Polym. Adv. Technol.*, 2018, **29**, 2816–2826.
47 G. Wang, W. Xu, R. Chen, W. Li, Y. Liu and K. Yang, *J. Appl. Polym. Sci.*, 2019, **137**, 48048.

48 L. Wan, C. Deng, H. Chen, Z. Y. Zhao, S. C. Huang, W. C. Wei, A. H. Yang, H. B. Zhao and Y. Z. Wang, *Chem. Eng. J.*, 2021, **417**, 129314.
49 Y. Yao, M. Xiao and W. Liu, *Macromol. Chem. Phys.*, 2021, **222**, 2100002.
50 K. Chen, M. Liu, Y. Shi, H. Wang, L. Fu, Y. Feng and P. Song, *Nano Res.*, 2022, **15**, 9531–9543.
51 M. Liu, K. Chen, Y. Shi, H. Wang, S. Wu, R. Huang, Y. Feng, L. Tang, X. Liu and P. Song, *J. Mater. Sci. Technol.*, 2023, **166**, 133–144.
52 W. Xu, Z. Cheng, D. Zhong, Z. Qin, N. Zhou and W. Li, *Polym. Adv. Technol.*, 2021, **32**, 2072–2081.
53 H. Li, D. Meng, P. Qi, J. Sun, H. Li, X. Gu and S. Zhang, *Appl. Clay Sci.*, 2022, **216**, 106376.
54 W. Wu, W. Huang, Y. Tong, J. Huang, J. Wu, X. Cao, Q. Zhang, B. Yu and R. K. Y. Li, *Appl. Surf. Sci.*, 2023, **610**, 155540.
55 B. Tu, K. Zhou, Q. Zhou, K. Gong and D. Hu, *RSC Adv.*, 2021, **11**, 9942–9954.
56 W. Xu, C. Cheng, Z. Qin, D. Zhong, Z. Cheng and Q. Zhang, *Polym. Adv. Technol.*, 2020, **32**, 228–240.
57 Y. Qian, W. Su, L. Li, R. Zhao, H. Fu, J. Li, P. Zhang, Q. Guo and J. Ma, *Polymers*, 2022, **14**, 2204.
58 Y. Geng, Z. Zhao, R. Li, X. Liu, G. Li, M. Wan, L. Liu, X. Chen and C. Jiao, *Polym. Degrad. Stab.*, 2024, **227**, 110845.
59 Y. Liang, H. Jian, C. Deng, J. Xu, Y. Liu, H. Park, M. Wen and Y. Sun, *Polymers*, 2023, **15**, 950.
60 Q. Li, X. Song, Y.-T. Pan, J. Sun, A. Bifulco and R. Yang, *J. Colloid Interface Sci.*, 2024, **674**, 445–458.
61 H. Wang, H. Qiao, J. Guo, J. Sun, H. Li, S. Zhang and X. Gu, *Composites, Part B*, 2020, **182**, 107498.
62 X. Chen, X. Chen, S. Li and C. Jiao, *Polym. Adv. Technol.*, 2021, **32**, 2829–2842.
63 Q. Liu, H. Wang, H. Li, J. Sun, X. Gu and S. Zhang, *Polym. Adv. Technol.*, 2022, **33**, 2374–2385.
64 M. Wan, C. Shi, X. Qian, Y. Qin, J. Jing, H. Che, F. Ren, J. Li, B. Yu and K. Zhou, *Chem. Eng. J.*, 2023, **459**, 141448.
65 C. Shi, M. Wan, X. Qian, H. Che and J. Li, *J. Therm. Anal. Calorim.*, 2024, **149**, 2777–2787.
66 Q. Yao, S. Li, J. Ban, B. Yang, T. Xu, H. Ren and Y. Huang, *ChemistrySelect*, 2024, **9**, e202401227.
67 G. W. Peterson, D. T. Lee, H. F. Barton, T. H. Epps and G. N. Parsons, *Nat. Rev. Mater.*, 2021, **6**, 605–621.
68 L. Chen, B. Huang, F. Wei, X. Guo, D. Zhang, K. Thummavichai, D. Chen, N. Wang and Y. Zhu, *ACS Appl. Polym. Mater.*, 2023, **5**, 9852–9864.
69 H. Wang, K. Chen, Y. Shi, Y. Zhu, S. Jiang, Y. Liu, S. Wu, C. Nie, L. Fu, Y. Feng and P. Song, *Chem. Eng. J.*, 2023, **474**, 145904.
70 H. Wang, Y. Jiang, Z. Ma, Y. Shi, Y. Zhu, R. Huang, Y. Feng, Z. Wang, M. Hong, J. Gao, L. C. Tang and P. Song, *Adv. Funct. Mater.*, 2023, **33**, 2306884.
71 M. Wan, C. Shi, X. Qian, Y. Qin, J. Jing, H. Che, F. Ren, J. Li and B. Yu, *Composites, Part A*, 2022, **163**, 107187.
72 C. Shi, M. Wan, Z. Hou, X. Qian, H. Che, Y. Qin, J. Jing, J. Li, F. Ren, B. Yu and N. Hong, *Polym. Degrad. Stab.*, 2022, **204**, 110119.
73 X. Bi, K. Song, Z. Zhang, T. Lin, Y.-T. Pan, W. Fu, P. Song, J. He and R. Yang, *Small*, 2024, 2403375, DOI: **10.1002/smll.202403375**.
74 M. Wan, C. Shi, L. Chen, L. Deng, Y. Qin, H. Che, J. Jing, J. Li and X. Qian, *Polym. Degrad. Stab.*, 2024, **226**, 110821.
75 N. V. Gama, A. Ferreira and A. Barros-Timmons, *Materials*, 2018, **11**, 1841.
76 A. Jaisingh, M. W. Halloran, B. S. Rajput and M. D. Burkart, *ACS Appl. Polym. Mater.*, 2024, **6**(16), 9724–9734.
77 M. Zhu, Z. Ma, L. Liu, J. Zhang, S. Huo and P. Song, *J. Mater. Sci. Technol.*, 2022, **112**, 315–328.
78 J. Cheng, D. Ma, S. Li, W. Qu and D. Wang, *Polymers*, 2020, **12**, 347.
79 W. Xu, G. Wang, J. Xu, Y. Liu, R. Chen and H. Yan, *J. Hazard. Mater.*, 2019, **379**, 120819.
80 C. Liang, W. Lin, Y. Liu, M. Kang, F. Zhang, W. Qu, S. Li and J. Cheng, *J. Therm. Anal. Calorim.*, 2023, **148**, 9511–9518.
81 K. Song, X. Bi, C. Yu, Y.-T. Pan, P. Xiao, J. Wang, J. I. Song, J. He and R. Yang, *ACS Appl. Mater. Interfaces*, 2024, **16**, 15227–15241.
82 J. Feng, L. Liu, Y. Zhang, Q. Wang, H. Liang, H. Wang and P. Song, *Exploration*, 2023, **3**, 20220088.
83 S. Makowska, D. Szymborski, N. Sienkiewicz and A. Kairytė, *Materials*, 2024, **17**, 3971.
84 D. Dukarska and R. Mirski, *J. Compos. Sci.*, 2024, **8**, 286.
85 G. Bo, X. Xu, X. Tian, J. Yan, X. Su and Y. Yan, *Polymers*, 2022, **14**, 3630.
86 X. Liu, P. Guo, B. Zhang and J. Mu, *Colloids Surf., A*, 2023, **671**, 131625.
87 P. M. Visakh, A. O. Semkin, I. A. Rezaev and A. V. Fateev, *Constr. Build. Mater.*, 2019, **227**, 116673.
88 Y. Geng, R. Li, Z. Zhao, G. Li, B. Huang, X. Chen and C. Jiao, *Chemosphere*, 2024, **357**, 142048.
89 H. Singh, N. Bhardwaj, S. K. Arya and M. Khatri, *Environ. Nanotechnol., Monit. Manage.*, 2020, **14**, 100305.
90 S. Zhao, L. Yin, Q. Zhou, C. Liu and K. Zhou, *Appl. Surf. Sci.*, 2020, **506**, 144700.
91 N. Habibi, S. Faraji and A. Pourjavadi, *Colloids Surf., A*, 2023, **676**, 132186.
92 Y. Hou, Z. Xu, Y. Yuan, L. Liu, S. Ma, W. Wang, Y. Hu, W. Hu and Z. Gui, *Compos. Sci. Technol.*, 2019, **177**, 66–72.
93 Y. Zhou, S. Qiu, F. Chu, W. Yang, Y. Qiu, L. Qian, W. Hu and L. Song, *J. Colloid Interface Sci.*, 2022, **609**, 794–806.
94 J. Piao, M. Lu, J. Ren, Y. Wang, T. Feng, Y. Wang, C. Jiao, X. Chen and S. Kuang, *J. Hazard. Mater.*, 2023, **444**, 130398.